IDENTIFICATION AND CONTROL OF LINEAR TIME-PERIODIC SYSTEMS VIA HARMONIC TRANSFER FUNCTIONS

DOĞRUSAL VE PERİYODİK ZAMANLI SİSTEMLERİN HARMONİK TRANSFER FONKSİYONLARI YARDIMIYLA SİSTEM TANIYIMI VE DENETİMİ

BAŞAK SERT

ASSOC. PROF. DR. İSMAİL UYANIK

Supervisor

Submitted to

Graduate School of Science and Engineering of Hacettepe University

as a Partial Fulfillment to the Requirements

for the Award of the Degree of Master of Science

in Electrical and Electronics Engineering

March 2023

ABSTRACT

IDENTIFICATION AND CONTROL OF LINEAR TIME-PERIODIC SYSTEMS VIA HARMONIC TRANSFER FUNCTIONS

Başak SERT

Master of Science, Electrical and Electronics Engineering

Supervisor: İsmail Uyanık

March 2023, 107 pages

The increased need for accurately modeling the input–output characteristics of linear time-periodic (LTP) systems necessitates novel identification and control algorithms as well as new test benches for their experimental validation. This thesis introduces a simple-to-build test bench for experimental identification and control of LTP systems both with time-invariant and time-varying controllers. We mechanically coupled the shafts of two DC motors and fed back the angular velocity to the second motor with a time-periodic modulation. This allowed us to imitate a time-periodic load for the first DC motor, thereby yielding an experimental LTP system plant. We used Matlab/Simulink target hardware support to implement the entire software in Simulink, which greatly simplifies input design, data collection, and analysis as compared to embedded programming. We used constant-frequency sinusoidal signals for the data collection on the experimental platform. Subsequently, we estimated the harmonic transfer functions and identified the parameters of a state-space model of the proposed LTP system. We then designed a time-periodic controller in order to regulate the output of the LTP system. We proposed a method for obtaining a linear time-periodic LQR controller in order to capture the time-varying dynamics of the systems.

In this research, we also employed the Mathieu equation as a representative example of a Linear Time Periodic (LTP) system for simulation purposes. We analyzed the equation both theoretically and using data-driven methods, and verified the results by comparing the output predictions from both methods. In previous research, most controllers used for analyzing the Mathieu equation were linear time-invariant. In contrast, in this thesis, we proposed the implementation of time-periodic controllers. Following this, we employed linear quadratic regulator (LQR) controllers in LTI and LTP forms to control the system and evaluated their performance through simulations in MATLAB/Simulink. We compared metrics such as root mean squared error (RMSE) and system characteristics, including overshoot and settling time. The effects of linear time-invariant (LTI) and linear time-periodic (LTP) type controllers on the dynamics of an LTP system have been investigated.

Keywords: Linear Time Periodic Systems, Harmonic Transfer Functions, System Identification, Time Periodic Experimental Test Bench, Time-Varying Systems Control, Motion Control of Dc Motors.

ÖZET

DOĞRUSAL VE PERİYODİK ZAMANLI SİSTEMLERİN HARMONİK TRANSFER FONKSİYONLARI YARDIMIYLA SİSTEM TANIYIMI VE DENETİMİ

Başak SERT

Yüksek Lisans, Elektrik ve Elektronik Mühendisliği

Danışman: İsmail UYANIK

Mart 2023, 107 sayfa

Doğrusal zamansal (LTP) sistemlerin giriş-çıkış özelliklerinin doğru bir şekilde modellenmesine yönelik artan ihtiyaç, yeni tanımlama ve kontrol algoritmalarının yanı sıra yeni deneysel test platformlarına duyulan ihtiyacı da arttırmaktadır. Bu tez doğrusal zamansal (LTP) sistemlerinin deneysel olarak tanımlanması ve hem zamanla değişmeyen, hem de zamanla değişen kontrolörlerle kontrolünün sağlanması için kurulumu basit bir test düzeneği sunmaktadır. İki DC motoru mil kısımlarından birbirine sabit bir şekilde bağlanmış ve ikinci motorun açısal hızı zamansal periodik bir sinyal olarak sisteme beslenmiştir. Bu işlem birinci motora zamansal periodik bir etki kazandırmış ve sonucunda zamansal periodik (LTP) bir sistem oluşmuştur. Matlab/Simulink tarafından sağlanan hedef donanım desteğini kullanarak (target hardware support) yardımı ile bütün yazılım Simulink ortamında gerçekleştirilmiştir. Simülasyon ortamını kullanmak girdi dizaynı, veri toplama ve analiz aşamalarında gömülü yazılıma kıyasla büyük kolaylık sağlamıştır. Deney sırasında sabit frekansta sinüs sinyalleri kullanarak Harmonik transfer fonksiyonlarınının (HTFs) analizi,

parametrik olmayan sistem tanıyım yöntemi ve bilinen bir durum uzay formunu kullanarak parametrik sistem tanıyım işlemleri gerçekleştirilmiştir.

Sistemlerin zamanla değişen dinamiklerini yakalamak için lineer zaman periyodik bir LQR kontrolör tasarımı önerilmiştir. Önerilen tasarım, hem simülasyon hem de LTP test platformunda doğrulanmıştır. Aynı zamanda bu araştırmada, Mathieu denklemi LTP (Lineer Zamansal Periodik) sistemlerin bir örneği olarak kullanılmıştır. Teorik olarak ve veri-tabanlı yöntemlerle Mathieu denklemi analiz edilmiş ve sonuçları veri-tabanlı ve teorik olarak hesaplanmıştır. Harmonik transfer fonksiyonları arasındaki çıktı tahminlerini karşılaştırarak çıktı analizleri gerçekleştirlmiş ve harmonik transfer fonksiyonlaru doğrulanmıştır. Önceki araştırmalarda, Mathieu denklemi için kullanılan kontrolörlerin çoğu lineer zamansal-değişmez yapıdadır. Bu tezde ise, zamansal-periodik kontrolörlerin tasarım ve uygulama sonuçlarına yer verilmiştir. Mathieu denkleminin durum uzayı formuna sahip olduğumuz için LTI ve LTP tipi LQR kontrolörler tasarlanmış ve sonuçları MATLAB/Simulink'teki simülasyonlarla doğrulanmıştır. Ayrıca ortalama hata kareleri toplamı kökü (RMSE) değerlerini karşılaştırarak LTI ve LTP tipi kontrolörlerin performans metriklerini verilmiştir. Lineer zamandan bağımsız(LTI) ve doğrusal zamansal periyodik (LTP) tipi kontrolörün, LTP sisteminin dinamikleri üzerindeki etkileri incelenmiştir.

Keywords: Doğrusal Zamanlı Periyodik Sistemler, Harmonik Transfer Fonksiyonları, Zamansal Değişen Sistemlerin Kontrolü, DC Motor Hareket Kontrolü, Sistem Tanımlama, Zamansal Periyodik Deney Platform Tasarımı,

ACKNOWLEDGEMENTS

Firstly, I would like to express my gratitude to my supervisor, Dr. İsmail UYANIK, for his guidance, encouragement, and continuous support throughout my study. He always encouraged and guided me through the learning process of my graduate education.

I am immensely grateful to Dr. Bahadır ÇATALBAŞ for his guidance and support throughout my thesis period. Also, I would like to thank the distinguished members of my thesis jury Dr. Hüseyin DEMİRCİOĞLU, Dr. Mustafa Mert ANKARALI, Dr. Şölen Kumbay YILDIZ, and Dr. Mahmud Derya ALTUNAY for approving my work and guiding me all the way up to this point. I am also indebted to all my instructors in undergraduate and graduate studies at Hacettepe University.

I am grateful to Ali Alperen BOŞNAK for his continuous support throughout my graduate education. He was always there to listen and motivate me.

Finally but forever, I owe my loving thanks to my parents Nuray-Yaşar SERT and my brother Cihan Ümit SERT for their undying love, support, and encouragement throughout my whole life.

CONTENTS

Page

TABLES

FIGURES

ABBREVIATIONS

LTI	:	**L**inear **T**ime **I**nveriant
LTP	:	**L**inear **T**ime **P**eriodic
EMP	:	**E**xponentially **M**odulated **P**eriodic
HTF	:	**H**armonic **T**ransfer **F**unction
PI	:	**P**roportional **I**ntegral
PD	:	**P**roportional **D**erivative
PID	:	**P**roportional **I**ntegral **D**erivative
LQR	:	**L**inear **Q**uadratic **R**egulator
p-LQR	:	**P**eriodic **L**inear **Q**uadratic **R**egulator
TV-LQR	:	**T**ime **V**arying **L**inear **Q**uadratic **R**egulator
ARE	:	**A**lgebraic **R**iccati **E**quation
DRE	:	**D**ifferential **R**iccati **E**quation
DRHBE	:	**D**ifferential **R**iccati **H**armonic **B**alance **E**quation
ODE	:	**O**rdinary **D**ifferential **E**quation
CPR	:	**C**ounts **P**er **R**evolution
PWM	:	**P**ulse **W**ith **M**odulation
RMSE	:	**R**oot **M**ean **S**quare **E**rror

1. INTRODUCTION

The analysis, identification, and control of periodic motion continuously gain more interest due to the increased need to accurately describe and regulate systems with periodic dynamics [1, 2], such as wind turbines [3, 4], power systems [5–7], and helicopter rotor dynamics [8–11]. In addition to these examples, periodic sampling of continuous-time systems [12] and linearization of nonlinear systems around a limit cycle introduce linear time-periodic (LTP) systems [13], which necessitate more than a classical linear time-invariant (LTI) analysis to successfully characterize their time-periodic nature.

The pioneering work of Mathieu, which dates back to the 1870s, on investigating the natural modes of vibration of lakes with elliptic boundaries led to the development of the first comprehensive theory on LTP systems [14]. Subsequently, Floquet established the foundations of stability analysis of periodic systems by proving the existence of a similarity transformation that generates a time-invariant state matrix [15]. Another milestone in the analysis of periodic systems was marked by the proposition of a linear operator—termed harmonic transfer functions (HTFs)— between the input and output of LTP systems [16]. HTFs model the input–output relationship of an LTP system via multiple (possibly infinite) modulated LTI transfer functions corresponding to each harmonic response of the LTP system. This representational power motivated the researchers to use HTFs as a reference model for the identification [11, 17] and control [18] of the periodic systems. The parametric structure of HTFs also led to the identification of state-space models for LTP systems using subspace identification [19].

The identification and control problems for LTP systems have vastly been studied in simulation except for a few notable works [8, 11, 20, 21]. We believe that a major reason behind this issue is the unavailability of simple, low-cost LTP system plants to experiment with. We found two promising directions to build a simple experimental LTP system plant. First, the mechanical coupling of two DC motors yields an LTP system plant, when one of the motors is driven with a sinusoidal input modulated by the angular velocity of the secondary

coupling motor [22]. Second, an inverted pendulum with a vertical periodic oscillation yields an LTP system plant [23]. To be more specific, these systems generate a limit cycle behavior, which turns into an LTP system plant when linearized around a periodic orbit.

In this thesis, we used two different LTP systems for the validation of our identification and control studies. First, we worked in simulation using the well-known Mathieu equation, a benchmark example used for LTP systems. Second, we developed a new experimental test bench to generate a physical LTP system for our experiments. First, we started by performing all identification and control techniques for the Mathieu equation. In order to study the LTP nature of the Mathieu equation, we employed a combination of theoretical and data-driven techniques. By utilizing cosine input signals of varying frequencies, we were able to gather input-output data from simulations in MATLAB/Simulink. This data was then used to estimate the Harmonic Transfer Functions (HTFs) of the system via Data-Driven Identification analyses. To evaluate the accuracy of our Data-Driven Identification HTFs estimation results, we compared the output prediction with the actual system output.

As a second LTP system example, motivated by [22], we mechanically coupled the shafts of two brushed DC motors to build an LTP system. We used Matlab/Simulink run-on-target-hardware support to prepare the software for the test setup in the Simulink environment. This allows input design, data collection, and analysis to be performed directly on Matlab/Simulink without dealing with the difficulties of embedded programming [24]. We used optical digital encoders on DC motors to measure the angular velocity. We then fed back this measurement by modulating it with a sinusoidal forcing function to obtain an LTP system plant.

We used analytical derivations and data-driven analysis to present the LTP nature of the proposed test bench. To achieve this, we first obtained the parametric LTP state-space model of the coupled DC motor system. We then used constant-frequency periodic excitations to estimate the harmonic transfer functions of the experimental test bench. Also, we performed a parametric system identification to estimate the unknown parameters in the state-space model. This enabled us to effectively design controllers offline and test them

in the simulation. Once the target metrics are attained, we deployed the controllers onto the test bench to assess their performance on a physical LTP system.

The objective of this thesis is to investigate and develop different system identification and controller design methodologies for LTP systems. For the system identification part, we mainly focused on harmonic transfer functions and parametric system identification. Previous studies have utilized different types of LTI controllers such as P-PD-PID controllers [25][16] for LTP systems. We offered a method for periodic controller design to capture also the periodic dynamics of the LTP systems and showed that the periodic controllers give better responses for LTP system control. In order to design controllers for LTP systems, various methodologies have been developed utilizing the state space model. A commonly employed controller for LTP systems is the Linear Quadratic Regulator (LQR) which aims to design a full state feedback control law that minimizes a quadratic cost function[26, 27]. The LQR gain is obtained by solving a Riccati differential equation, thereby providing an optimal controller that increases the robustness of the system and ensures the closed-loop stability of the LTP system. For Linear Time-Varying (LTV) systems, the cost function and control law must be adjusted to account for the time-varying nature of the system. This can be achieved by formulating the cost function and control law as a function of time. The Time-Varying LQR (TV-LQR) method involves solving the LQR problem at each time instant using the system's current state and the system's model at that time. However, solving the Riccati differential equation to achieve optimal feedback gain can be a challenging task due to the complexity of the matrices involved. To overcome this, a method of converting the Ricatti matrices to all real-valued matrices has been proposed for ease of mathematical calculations. Additionally, powerful tools such as MATLAB can be utilized to solve the Ricatti equations. For our analysis, since the system matrices are known, the Toeplitz form LQR controllers were designed using offline methods and converted to the periodically varied time domain K_{LQR} gains. Once the stability and performance of the controllers were validated through simulation, they were implemented on the Mathieu equation and after that, they were deployed onto the physical LTP system using time-periodic K_{LQR} gains. This allowed us to move from the simulation environment to real-world implementation

and ensured that both the frequency and time domains of the system were improved. Also, two different references tracking LQR architectures had been proposed, namely the Linear Quadratic Integrator and LQR with precompensator gain. The tracking performance of the LTP systems was evaluated using the Root Mean Square Error (RMSE) between the reference signal and system responses.

1.1. Key contributions of this thesis

In this research, a significant advancement in the field of developing physical test platforms and control systems for linear time-periodic systems was achieved by:

1. Introducing the design steps of a simple-to-build physical LTP system plant with Matlab/Simulink run-on-target-hardware support

2. Utilizing system identification methods in order to derive a Harmonic Transfer Function model for the Mathieu equation and the coupled DC motor platform. This is accomplished through the implementation of both data-driven and novel parametric identification techniques to identify the state-space model and unknown system parameters of the LTP platform.

3. This thesis offers a method for time-periodic LQR controller design for LTP systems. The primary objective is to use this method to create periodic LQR controllers, which can be employed in different reference tracking structures. The proposed control approach is tested through simulations conducted on different LTP system models, including the Mathieu equation, as well as on a physical LTP test platform that has been created in-house, unlike other applications on simulations testing them on a physical test bench. The main goal is to evaluate the efficacy of the control method in order to determine its suitability for the intended application.

1.2. Organization of this thesis

The structure of the thesis is arranged as follows:

- Chapter 1 presents the introduction and the scope of the thesis.
- Chapter 2 provides a background overview of the LTI and LTP systems and the Harmonic transfer function concept.
- Chapter 3 demonstrates the details of Linear Time Periodic simulation and physical test platforms.
- Chapter 4 gives an explanation of System Identification Techniques for an LTP system and gives the identification results for both the Mathieu equation and the physical test platform.
- Chapter 5 introduces controller design methodologies for both time-invariant and time-periodic nature. This chapter also offers a periodic Linear Optimal Quadratic Controller design and contains LQR controller basics. In the last part, the related validation results are introduced and compared with LTI and LTP-type controllers.
- Chapter 6 states the summary of the thesis and possible future directions.

2. BACKGROUND OVERVIEW

This chapter begins by discussing the overview of LTI systems and continues with explanations of linear time-varying systems, particularly linear time-periodic (LTP) systems, the concept of harmonic balance, and harmonic transfer functions.

2.1. Overview of LTI Systems

Linear time-invariant (LTI) systems are systems that possess two key features in input–output behavior: linearity and time-invariance. Linearity dictates homogeneity and superposition between the input and output signals. Time-invariance implies that the system's response is invariant to the time of operation. Namely, if the input is delayed (or time-advanced), the output will be in the same form with the same amount of delay (or time advance).

The state-space representation of an LTI system is given as

$$\begin{aligned} \dot{x}(t) &= Ax(t) + Bu(t) \\ y(t) &= Cx(t) + Du(t) \end{aligned} \tag{1}$$

where $A \in \mathbb{R}^{n\times n}$, $B \in \mathbb{R}^{n\times m}$, $C \in \mathbb{R}^{p\times n}$, and $D \in \mathbb{R}^{p\times m}$ are constant system matrices.

The Laplace transform of Eq. (1) and setting the initial condition $x(0) = 0$ the output is equal to

$$Y(s) = G(s)U(s) \tag{2}$$

and the transfer function is

$$G(s) = C(sI - A)^{-1}B + D \tag{3}$$

In all equations, I defines the identity matrix with proper dimension.

2.2. Linear Time Periodic Systems

In contrast to LTI systems, linear time-periodic (LTP) systems, which are a subclass of time-varying systems, exhibit varying behavioral responses over time. While LTI systems are simpler and more commonly found in various fields, the modeling of LTP systems is necessary for certain situations such as systems with time-varying parameters, time delays, or systems that are affected by external factors that alter their behavior over time.

Examples of LTP systems can be found in various fields such as mechanical systems, electrical systems, robotics, and orbital mechanics. For instance, a pendulum exhibits LTP characteristics due to its periodic dynamics [28]. Similarly, a power system can be considered an LTP system [5, 29]. In the field of robotics, many systems such as walking robots have a fixed periodic frequency and can be modeled as LTP systems[13]. Additionally, celestial bodies like satellites, moons, and comets experience nonlinear gravitational fields that can be linearized around a periodic orbit, making them examples of LTP systems [30].

LTP systems can be modeled and analyzed using mathematical models such as differential equations, state-space models, or harmonic transfer functions. The control of LTP systems can be more challenging than LTI systems due to their unique, challenging dynamics and may require the use of specialized control methods such as time-varying control, adaptive control, and robust control.

2.3. Frequency Response of LTP Systems

The linear time-periodic (LTP) systems are a subclass of time-varying systems in the form

$$\begin{aligned} \dot{x}(t) &= A(t)x(t) + B(t)u(t) \\ y(t) &= C(t)x(t) + D(t)u(t) \end{aligned} \tag{4}$$

where $A(t) \in \mathbb{R}^{n\times n}$, $B(t) \in \mathbb{R}^{n\times m}$, $C(t) \in \mathbb{R}^{p\times n}$, and $D(t) \in \mathbb{R}^{p\times m}$ are all periodic with a common period, T.

Unlike the SISO LTI systems, the frequency response of LTP systems can not be represented with a single input-output transfer function. The analysis of LTI systems greatly owes its success and maturity to the fact that sinusoidal signals serve as the eigenfunctions of the LTI systems. In the case of an LTP system, when a sinusoidal input is applied at a certain frequency (ω), the output (at the steady-state) does not only occur at the input frequency but also in the harmonics of the periodic frequency of the LTP system, $\omega_p = 2\pi/T$. Thus, the steady-state response of an LTP system to a sinusoidal input is the superposition of multiple (possibly infinite) modulated sinusoidal signals.

In the frequency domain, LTI systems have a one-to-one mapping between the frequency contents of the input and output signals. However, in LTP systems this corresponds to a one-to-many mapping between the frequency contents of the input and output signals. The frequency response characteristics are given in Fig. 2.1.

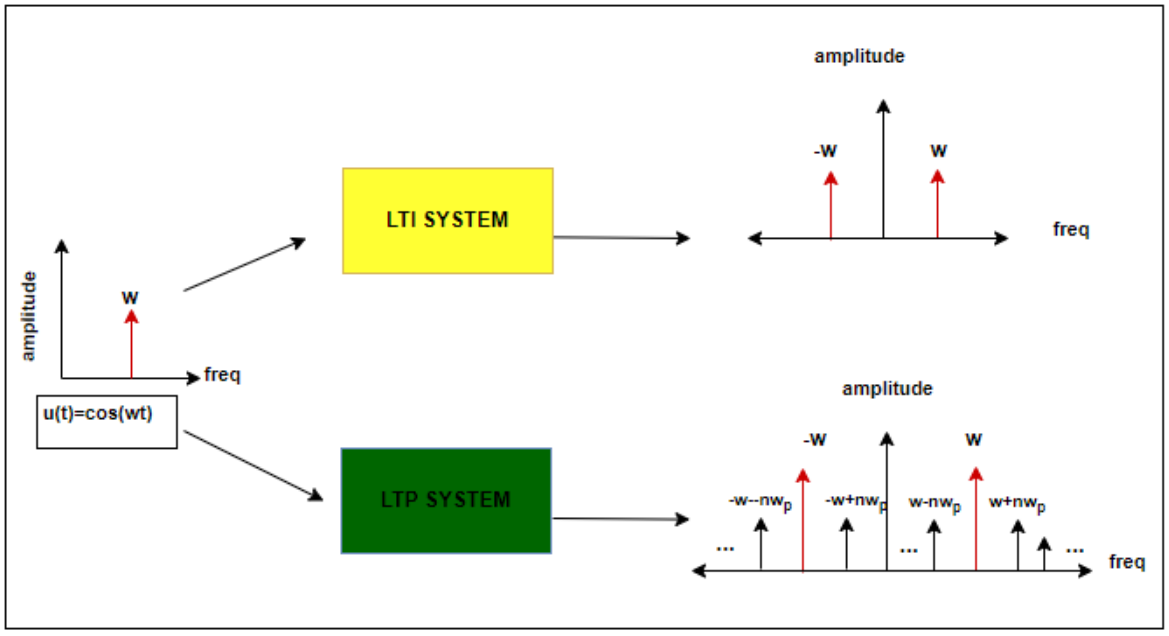

Figure 2.1 The response of the LTP and LTI systems to the specific frequency (w) cosine input signal. LTI systems give a response in the input frequency with possibly different amplitude and the LTP system gives a response in both the input frequency and also in the harmonics of the periodic frequency with possibly different amplitude.

Wereley proposed the concept of harmonic transfer functions (HTFs) to capture the characteristics of the frequency response functions of the LTP systems [31]. The basic

motivation behind the HTFs is to lift the LTP system to a higher dimensional LTI framework, where each harmonic response is represented with a distinct modulated transfer function. This lifted LTI representation of an LTP system allows us to utilize stability analysis and controller design techniques from LTI systems, of course with necessary modifications [32, 33].

The exponentially modulated periodic (EMP) complex signal concept is also introduced by Wereley [31] as an eigenfunction for the LTP systems, to introduce frequency response characteristics for LTP systems. The EMP signals are in the form of the sum of complex Fourier series of a periodic signal with the fundamental, or periodic, frequency, ω_p, as

$$u(t) = \sum_{n=-\infty}^{\infty} u_n e^{s_n t} \ , \tag{5}$$

where $s_n = s + jn\omega_p$ and $t \geq 0$. In the EMP signal domain, the states and steady-state output of the LTP system are also represented in the form of EMP signals as

$$x(t) = \sum_{n=-\infty}^{\infty} x_n e^{s_n t}, \ \ y(t) = \sum_{n=-\infty}^{\infty} y_n e^{s_n t} \tag{6}$$

Likewise, the state matrix, as well as the other state-space matrices, can be expressed in a similar form using their Fourier series coefficients as

$$A(t) = \sum_{n=-\infty}^{\infty} A_n e^{jn\omega_p t}. \tag{7}$$

$$B(t) = \sum_{n=-\infty}^{\infty} B_n e^{jn\omega_p t}, \tag{8}$$

$$C(t) = \sum_{n=-\infty}^{\infty} C_n e^{jn\omega_p t}. \tag{9}$$

$$D(t) = \sum_{n=-\infty}^{\infty} D_n e^{jn\omega_p t}. \tag{10}$$

The derivation of HTFs starts by plugging the EMP and Fourier series expansions back into Eq. (4) as

$$\begin{aligned}\sum_{n=-\infty}^{\infty} s_n x_n e^{s_n t} &= \textstyle\sum_{n=-\infty}^{\infty} A_n e^{jn\omega_p t} \sum_{m=-\infty}^{\infty} x_m e^{s_m t} \\ &+ \textstyle\sum_{n=-\infty}^{\infty} B_n e^{jn\omega_p t} \sum_{m=-\infty}^{\infty} u_m e^{s_m t}\end{aligned} \tag{11}$$

Simplifying Eq. (11) by combining the nested summations, we obtain

$$\sum_{n=-\infty}^{\infty} s_n x_n e^{s_n t} = \sum_{m,n=-\infty}^{\infty} A_{n-m} e^{s_n t} x_m + \sum_{m,n=-\infty}^{\infty} B_{n-m} e^{s_n t} u_m. \tag{12}$$

Likewise, we obtain the output equation as

$$\sum_{n=-\infty}^{\infty} y_n e^{s_n t} = \sum_{m,n=-\infty}^{\infty} C_{n-m} e^{s_n t} x_m + \sum_{m,n=-\infty}^{\infty} D_{n-m} e^{s_n t} u_m. \tag{13}$$

Combining all terms in Eq. (12) and Eq. (13) in one side yields

$$\begin{aligned} 0 &= \textstyle\sum_{n=-\infty}^{\infty} \left\{ s_n x_n - \sum_{m=-\infty}^{\infty} A_{n-m} x_m - \sum_{m=-\infty}^{\infty} B_{n-m} u_m \right\} e^{s_n t} \\ 0 &= \textstyle\sum_{n=-\infty}^{\infty} \left\{ y_n \quad - \sum_{m=-\infty}^{\infty} C_{n-m} x_m - \sum_{m=-\infty}^{\infty} D_{n-m} u_m \right\} e^{s_n t} \end{aligned} \tag{14}$$

The representation in (14) contains a special highlight that simplifies the analysis of the infinite summations. In (14), the modulation functions $e^{s_n t}$ constitute an orthogonal basis for each value of n. Therefore, the terms within the curly braces should be equal to zero for each n to make the infinite sum vanish, yielding

$$\begin{aligned} s_n x_n &= \textstyle\sum_{m=-\infty}^{\infty} A_{n-m} x_m + \sum_{m=-\infty}^{\infty} B_{n-m} u_m \\ y_n &= \textstyle\sum_{m=-\infty}^{\infty} C_{n-m} x_m + \sum_{m=-\infty}^{\infty} D_{n-m} u_m \end{aligned} \tag{15}$$

This is known as the harmonic balance principle. The equations in (15) give a clear description of the Fourier coefficients of input-output signals. To represent infinite summations via matrix operations, the Toeplitz transform should be used. The Toeplitz

transform can help to simplify algebraic operations involving sums and products of complex Fourier series. Also, it helps to transform time-periodic system differential equations into infinite-dimensional time invariant equations so the LTP system can be modeled as an endlessly large LTI system. As a result, the system equations in (15) can be expressed more briefly as

$$\begin{aligned} {}_s\mathcal{X} &= (\mathcal{A}-\mathcal{N})\mathcal{X}+\mathcal{B}\mathcal{U} \\ \mathcal{Y} &= \mathcal{C}\mathcal{X}+\mathcal{D}\mathcal{U} \end{aligned} \tag{16}$$

In Eq. (16) state vectors, input and output can be defined by doubly infinite matrices as

$$\mathcal{X}(s)=\left[\begin{array}{c} \cdots, x_{-1}^T(s), x_0^T(s), x_1^T(s)\cdots \end{array}\right]^T \tag{17}$$

$$\mathcal{U}(s)=\left[\begin{array}{c} \cdots, u_{-1}^T(s), u_0^T(s), u_1^T(s)\cdots \end{array}\right]^T \tag{18}$$

$$\mathcal{Y}(s)=\left[\begin{array}{c} \cdots, y_{-1}^T(s), y_0^T(s), y_1^T(s)\cdots \end{array}\right]^T \tag{19}$$

Also, T-periodic system matrices have the same Teoplitz matrices form,

$$\mathcal{A}=\left[\begin{array}{ccccc} & \vdots & \vdots & \vdots & \vdots & \\ \cdots & A_0 & A_{-1} & A_{-2} & A_{-3} & \cdots \\ \cdots & A_1 & A_0 & A_{-1} & A_{-2} & \cdots \\ \cdots & A_2 & A_1 & A_0 & A_{-1} & \cdots \\ \cdots & A_3 & A_2 & A_1 & A_0 & \cdots \\ & \vdots & \vdots & \vdots & \vdots & \end{array}\right] \tag{20}$$

$B(t)$, $C(t)$, and $D(t)$ have the same Toeplitz form representation which involves their complex Fourier coefficients as

$$\mathcal{B} = \begin{bmatrix} & \vdots & \vdots & \vdots & \vdots & \\ \cdots & B_0 & B_{-1} & B_{-2} & B_{-3} & \cdots \\ \cdots & B_1 & B_0 & B_{-1} & B_{-2} & \cdots \\ \cdots & B_2 & B_1 & B_0 & B_{-1} & \cdots \\ \cdots & B_3 & B_2 & B_1 & B_0 & \cdots \\ & \vdots & \vdots & \vdots & \vdots & \end{bmatrix} \tag{21}$$

$$\mathcal{C} = \begin{bmatrix} & \vdots & \vdots & \vdots & \vdots & \\ \cdots & C_0 & C_{-1} & C_{-2} & C_{-3} & \cdots \\ \cdots & C_1 & C_0 & C_{-1} & C_{-2} & \cdots \\ \cdots & C_2 & C_1 & C_0 & C_{-1} & \cdots \\ \cdots & C_3 & C_2 & C_1 & C_0 & \cdots \\ & \vdots & \vdots & \vdots & \vdots & \end{bmatrix} \tag{22}$$

$$\mathcal{D} = \begin{bmatrix} & \vdots & \vdots & \vdots & \vdots & \\ \cdots & D_0 & D_{-1} & D_{-2} & D_{-3} & \cdots \\ \cdots & D_1 & D_0 & D_{-1} & D_{-2} & \cdots \\ \cdots & D_2 & D_1 & D_0 & D_{-1} & \cdots \\ \cdots & D_3 & D_2 & D_1 & D_0 & \cdots \\ & \vdots & \vdots & \vdots & \vdots & \end{bmatrix} \tag{23}$$

and N is a block-diagonal matrix. The Toeplitz form representation of N is given as

$$\mathcal{N} = \begin{bmatrix} & \vdots & \vdots & \vdots & \vdots \\ \cdots & -jnw_0 I & 0 & 0 & \cdots \\ \cdots & 0 & -jnw_0 I & 0 & \cdots \\ \cdots & 0 & 0 & -jnw_0 I & \cdots \\ & \vdots & \vdots & \vdots & \vdots \end{bmatrix} \tag{24}$$

where I is the identity matrix with the proper dimension.

A detailed derivation can be found in [16]. Once the doubly-infinite state-space matrices are constructed (see Section 2.4.), the input-output relationship can be obtained as

$$\mathcal{Y}(s) = \mathcal{H}(s)\mathcal{U}(s) \ , \tag{25}$$

where the harmonic transfer functions, $H(s)$ can be computed as

$$H(s) = \mathcal{C}[s\mathcal{I} - (\mathcal{A} - \mathcal{N})]^{-1}\mathcal{B} + \mathcal{D}. \tag{26}$$

Here, HTFs are also in a doubly infinite (semi)-Toeplitz matrix form as

$$\mathcal{H}(s) = \begin{bmatrix} & \vdots & \vdots & \vdots & \vdots & \vdots & \\ \cdots & H_0(s-j2\omega_p) & H_{-1}(s-j\omega_p) & H_{-2}(s) & H_{-3}(s+j\omega_p) & H_{-4}(s+j2\omega_p) & \cdots \\ \cdots & H_1(s-j2\omega_p) & H_0(s-j\omega_p) & H_{-1}(s) & H_{-2}(s+j\omega_p) & H_{-3}(s+j2\omega_p) & \cdots \\ \cdots & H_2(s-j2\omega_p) & H_1(s-j\omega_p) & H_0(s) & H_{-1}(s+j\omega_p) & H_{-2}(s+j2\omega_p) & \cdots \\ \cdots & H_3(s-j2\omega_p) & H_2(s-j\omega_p) & H_1(s) & H_0(s+j\omega_p) & H_{-1}(s+j2\omega_p) & \cdots \\ & \vdots & \vdots & \vdots & \vdots & \vdots & \end{bmatrix} \tag{27}$$

The relationship between the input and output signals of the LTP system can be modeled with HTFs as in Eq. (27). In this equation ω_p is the periodic frequency generally (rad/sec),

$H_{\pm i}(s)$ represents the harmonic transfer function that gives the relationship between input and output at frequency ω.

The relationship between input and output in LTP systems can be represented by several LTI subsystems. The illustration of that property can be found in Fig. 2.2.

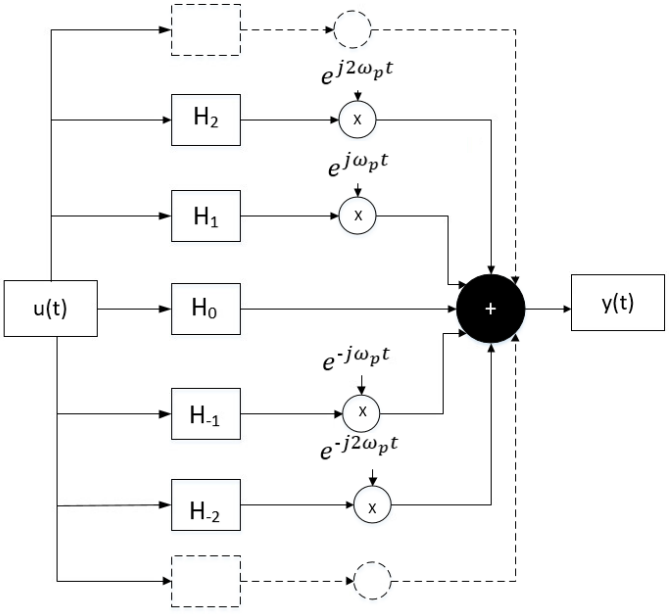

Figure 2.2 HTF structure representation of the LTP system. LTP systems can be represented by a set of lifted LTI subsystems.

2.4. Truncation of LTP Frequency Responses

In practical applications, the use of a finite number of harmonic transfer functions is necessary for computational feasibility on digital computers. However, truncation can also introduce errors and approximations, which can have effects on the overall system's performance. The effects of truncation of an LTP system depend on the number of terms removed and the importance of those terms to the overall system behavior. The number of harmonics to be used is mostly determined with a guess after observing the frequency content of the output data. To bring the system into the harmonic balance form, we need to compute the Fourier series coefficients of the system matrices.

Assume that we only have a time-periodic component in the state matrix $A(t)$ matrix. Thus, we need to compute the Fourier series coefficients of the matrix $A(t)$. Since only the DC component (fundamental harmonic) and first harmonic at ω_p have a noticeable effect in the LTP formulation, we truncated the Toeplitz matrix such that we have 6×6 A_i, where $i = -1, 0, 1$ as

$$A(t) = \sum_{n=-\infty}^{\infty} A_n e^{jn\omega_p t} = \sum_{n=-1}^{1} A_n e^{jn\omega_p t} \tag{28}$$

and the following related truncated Toeplitz form of A matrix

$$A(s) = \begin{bmatrix} & \vdots & \vdots & \vdots & \vdots \\ \cdots & A_0 & A_{-1} & Z_0 & \cdots \\ \cdots & A_1 & A_0 & A_{-1} & \cdots \\ \cdots & Z_0 & A_1 & A_0 & \cdots \\ & \vdots & \vdots & \vdots & \vdots \end{bmatrix} \tag{29}$$

with Z_0 is the zero matrices of the same dimension as A_i. After the truncation is performed, the eigenlocus is given in Fig. 2.3.

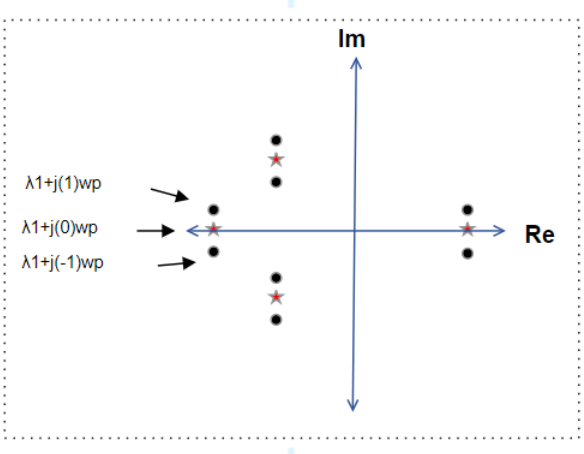

Figure 2.3 Eigenvalue loci of a truncated harmonic number n=1 LTP system: red⋆- significant eigenvalues; black -periodic eigenvalues of the system

3. SIMULATION ENVIRONMENT AND EXPERIMENTAL TEST BENCH

A majority of current research on LTP systems uses simulation models for practical applications. In this thesis, we aimed to contribute to the field of LTP systems by first developing a physical test platform that allows experimental investigation of our approaches. Furthermore, we used the well-known Mathieu equation for benchmarking in simulation to make a fair comparison with the existing literature.

The physical experimental test bench was used to observe the behavior of LTP systems under different operating conditions and with different controllers, LTI or LTP. The specifics of our simulation environment and the experimental test bench are outlined in the following sections.

3.1. Mathieu Equation as an LTP System Model

The Mathieu equation, developed by Émile Mathieu, is a well-known ordinary differential equation (ODE) that possesses LTP system dynamics [34]. First introduced by Mathieu's equation for the analysis of vibrations in an elliptic drum membrane, this equation is an example of Hill's equation, which describes the motion of a system subject to a periodically varying force. In addition to vibration theory, the Mathieu equation is widely used in various fields of applied mathematics, physics, and engineering, such as ship and train stability [35], quantum mechanical systems [36], and the periodic motion of electrons in crystal lattices [37]. The following chapter provides a brief overview of the Mathieu equation and its derivatives.

3.1.1. Theoretical Analysis of Mathieu Equation

A single-degree-of-freedom Mathieu system was used to evaluate the proposed techniques and controllers in the simulation environment. The basic scheme of a sample Mathieu system

can be seen in Fig. 3.1 in the form of a spring-mass-damper system, where the spring stiffness is time-periodic. Another significant and widely used example of the Mathieu equation is the dynamics of an inverted pendulum, specifically, when there are oscillations of small amplitudes.

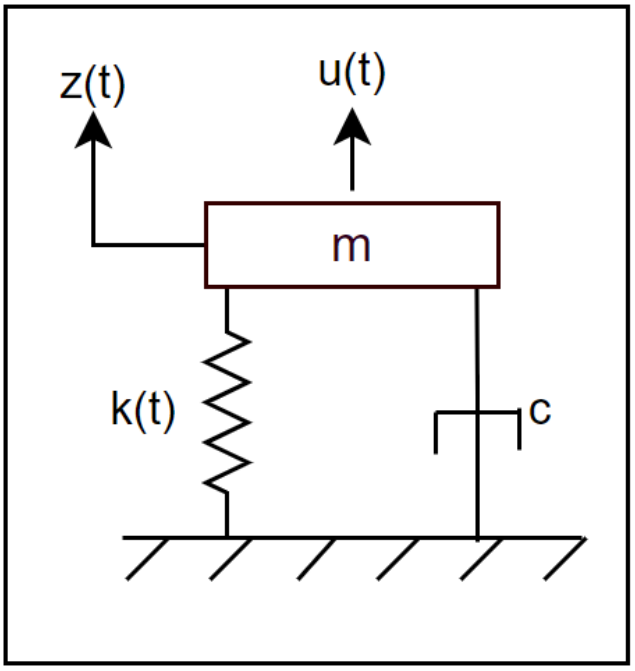

Figure 3.1 Mathieu system with a time-varying spring stiffness.

The Mathieu system has a constant mass (m) and damping (c) but the spring stiffness for the system varies periodically with frequency ω_p according to Eq. (30) as

$$k(t) = k_1 + k_2 \cos(\omega_p t) \tag{30}$$

The canonical form of the Mathieu equation is as

$$\ddot{z}(t) + 2\zeta w_n \dot{z}(t) + (1 + 2\beta cos w_p t) {w_n}^2 z(t) = \frac{u(t)}{m} \tag{31}$$

with $2\zeta\omega_n = c/m, \omega_n^2 = k_1/m, 2\omega_n^2\beta = k_2/m$ and $u(t)$ is the input signal. The states are displacement, z, and velocity, $\dot{z}$. Also, the state variables of the Mathieu equation are

$$\begin{aligned} z_1(t) &= z(t) \ , \\ z_2(t) &= \dot{z_1}(t) = \dot{z}(t) \ , \\ \dot{z}_2(t) &= \dot{z}_1(t) = \ddot{z}(t) \ . \end{aligned} \tag{32}$$

In Eq. (31) β defines the significance of the periodic effects. Specifically, when β is close to zero, the behavior is closer to an LTI system, while when the β is large, the impact of periodic harmonics becomes larger in the output (deviating from LTI behavior).

The state-space representations of system matrices of Eq. (31) are

$$A(t) = \begin{bmatrix} 0 & 1 \\ -(1 + 2\beta cos(w_p t){w_n}^2) & -2\zeta w_n \end{bmatrix} \tag{33}$$

$$B = \begin{bmatrix} 0 \\ 1 \end{bmatrix}, C = \begin{bmatrix} 1 & 0 \end{bmatrix} \tag{34}$$

The harmonic coefficients of the system matrices $A(t)$ are

$$A_0 = \begin{bmatrix} 0 & 1 \\ {w_n}^2 & -2\zeta w_n \end{bmatrix} \tag{35}$$

$$A_1 = \begin{bmatrix} 0 & 0 \\ -\beta {w_n}^2 & 0 \end{bmatrix} \tag{36}$$

$$A_{-1} = A_1 \tag{37}$$

The system matrices B and C have no periodic elements, and hence they do not generate higher harmonic matrices. Once these system matrices are obtained, one can easily calculate the harmonic transfer functions as will be later discussed in Sec. 4.

3.2. A New Experimental Test Platform to Study Linear Time-Periodic (LTP) Systems

One of the key contributions of this thesis is the design and development of a physical test platform that possesses LTP system dynamics. The construction of this physical test platform aims to study, analyze and improve the performance of these systems in a physical environment. The test bench comprises hardware components such as encoders, motors, motor drivers and etc., as well as software for data collection and analysis. It is utilized to evaluate the system under various operating conditions and to develop various control strategies to control and also capture the periodic nature of the LTP system. The ultimate goal is to acquire a deeper understanding of the behavior of LTP systems on a physical platform and enhance their performance. In this section, we first provide a description of the periodic nature of the experimental test bench. Then, we proceed to explain the technical characteristics of the test bench, including the hardware, electronic, and software components used.

3.2.1. LTP nature of the proposed test bench

The experimental test bench involves two mechanically-coupled DC motors with rigid connections, where one of them serves as the load to generate time-periodic system dynamics. To achieve periodicity in the experimental bench, we fed back the angular velocity of the coupled motor shafts to the load motor by modulating it with a sinusoidal signal. This way, the load motor plays the role of a linear time-periodic system plant as seen by the terminals of the first DC motor. An illustration of the proposed test bench is given in Fig. 3.2. In this experimental test bench, the two equal-weight loads are mechanically coupled between the two DC motors. The two identical DC motors have the same angular velocity, $\dot{\theta}$, and acceleration, $\ddot{\theta}$.

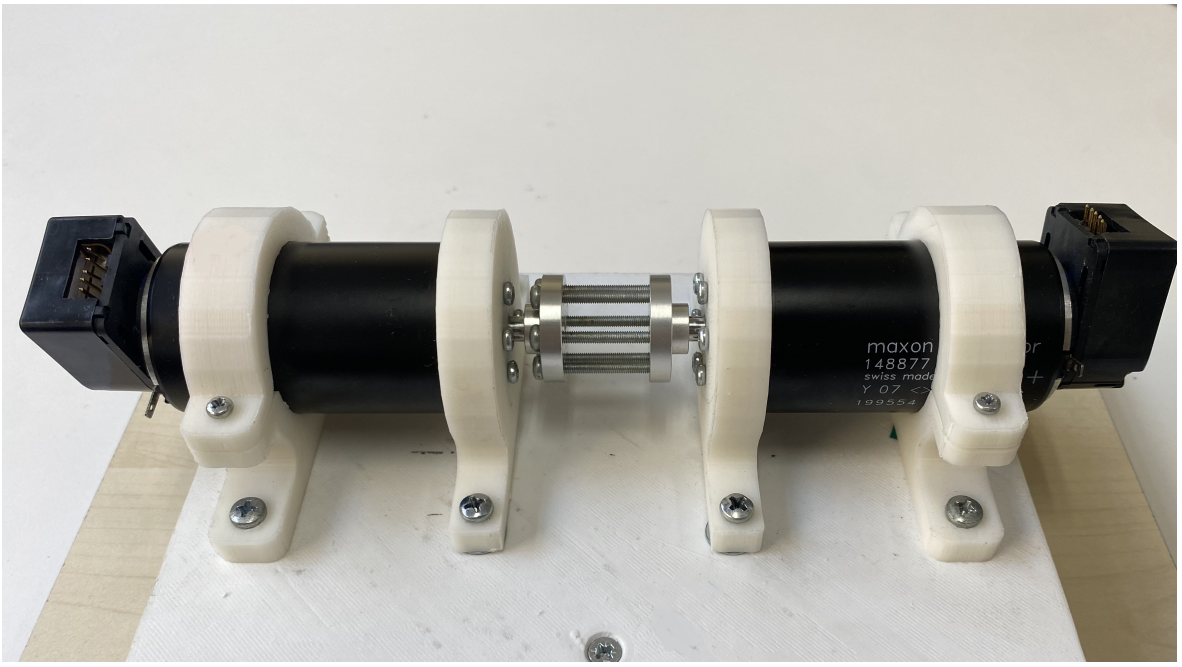

Figure 3.2 An illustration of the proposed LTP test bench. The DC motors are mechanically coupled with rigid connections. The periodic system nature is achieved by feeding back to the angular velocity to the load motor via periodic modulation.

The load motor is supplied with feedback of the angular velocity, modulated by a periodic input as

$$u_2(t) = -(F_0 + F_1 \cos(\omega_p t))\dot{\theta} \ , \tag{38}$$

where $F_0 = 0.055$, $F_1 = 0.045$ and periodic frequency $\omega_p = 4\pi$ rad/s.

Given this coupling and with periodic load, the system between the input terminals of the first DC motor and the outputs as an angular velocity admits the state-space form given in

(46) with state, input, and output matrices are given below,

$$\begin{aligned} A(t) &= \begin{bmatrix} 0 & 1 \\ \frac{-B_m}{T_m J} - \frac{K}{T_m J}(F_0 + F_1 cos(w_p t)) & \frac{-B_m}{J} - \frac{1}{T_m} \end{bmatrix} \\ B(t) &= \begin{bmatrix} 0 \\ \frac{K}{T_m J} \end{bmatrix} \\ C(t) &= \begin{bmatrix} 1 & 0 \end{bmatrix} \\ D(t) &= 0 \end{aligned} \tag{39}$$

and the full state-space representation of the system takes the form as

$$\begin{bmatrix} \ddot{\theta} \\ \dddot{\theta} \end{bmatrix} = \begin{bmatrix} 0 & 1 \\ \frac{-B_m}{T_m J} - \frac{K}{T_m J}(F_0 + F_1 cos(w_p t)) & \frac{-B_m}{J} - \frac{1}{T_m} \end{bmatrix} \begin{bmatrix} \dot{\theta} \\ \ddot{\theta} \end{bmatrix} + \begin{bmatrix} 0 \\ \frac{K}{T_m J} \end{bmatrix} u_1(t) \tag{40}$$

and the output equation of the velocity output-based system is

$$y(t) = \begin{bmatrix} 1 & 0 \end{bmatrix} \begin{bmatrix} \dot{\theta} \\ \ddot{\theta} \end{bmatrix} \tag{41}$$

where K, T_m, J, and B_m are intrinsic DC motor parameters that need to be and will be estimated using input–output data. More details about the state-space derivation can be found in [22].

3.2.2. Hardware Platform

In this part, we present the hardware specifications of the experimental test bench that enables us to perform the system identification techniques and control experiments for an LTP system. For this purpose, we used a microcontroller and two DC motor drivers to generate control signals for the DC motors and measure their angular velocity and for some processes,

the angular position was used as the output signal. Specifically, we employ two gearless Maxon DC motors (148877), which are equipped with HEDS-5540 high-precision optical incremental quadrature encoders with 500 counts per rotation (see Table 3.1 for hardware details). The encoder is mounted on one of the DC motors and utilized to measure the rotation of the coupled shafts of the DC motors. Thus, we can observe the angular position and speed of the coupled DC motor system. As DC motor driver, we use two IBT-2 H-Bridge modules based on two BTS7960 chips, which support pulse with modulation (PWM) frequency up to $25\ KHz$, supply voltages between $6 - 27\ V$, and drive currents up to $43\ A$.

Arduino Uno microcontroller boards have a wide usage area and familiarity between developers from various backgrounds as a low-cost solution. Benefiting from PWM outputs, interrupt inputs, and universal asynchronous receiver transmitter (UART) modules of the microcontrollers in the board, it is possible to use them effectively in control applications such as the design of undergraduate-level feedback control system course laboratory experiment kits [24]. Moreover, it is possible to program Arduino with a block diagram-based programming approach in the Simulink by the help of its hardware support package. Although there are various embedded solutions with greater processing power, a higher number of input and output pins, and Simulink and Matlab Embedded Coder support, we selected the Arduino Uno microcontroller board for our application due to its low cost and wide global usage experience areas.

Table 3.1 Hardware of LTP test bench

Hardware	**Amount**
Gearless Maxon DC motors (148877)	2
HEDS-5540 high-precision optical incremental quadrature encoders	2
DC motor drivers(IBT-2 H-Bridge modules based on two BTS7960 chips)	2

3.2.3. Software Platform

In the software design decisions, we prioritized the widespread use of the selected software both in the academy and industry. Besides, the proposed solution should allow a quick

adaptation to new experiments. In this context, block diagram-based programming is preferred thanks to the ease of use, familiarity in the field, and avoidance of dealing with the details of embedded programming. Under these requirements, Matlab promises a convenient solution with Control System Toolbox and Simulink environment, besides other toolboxes and libraries. One of these, the Simulink Support Package for Arduino Hardware library, enables us to design and maintain communications between Simulink models to Arduino boards, such as shown in Fig. 3.4. Furthermore, Matlab Embedded Coder can generate C/C++ codes for user-defined blocks in the Simulink environment according to the target embedded system.

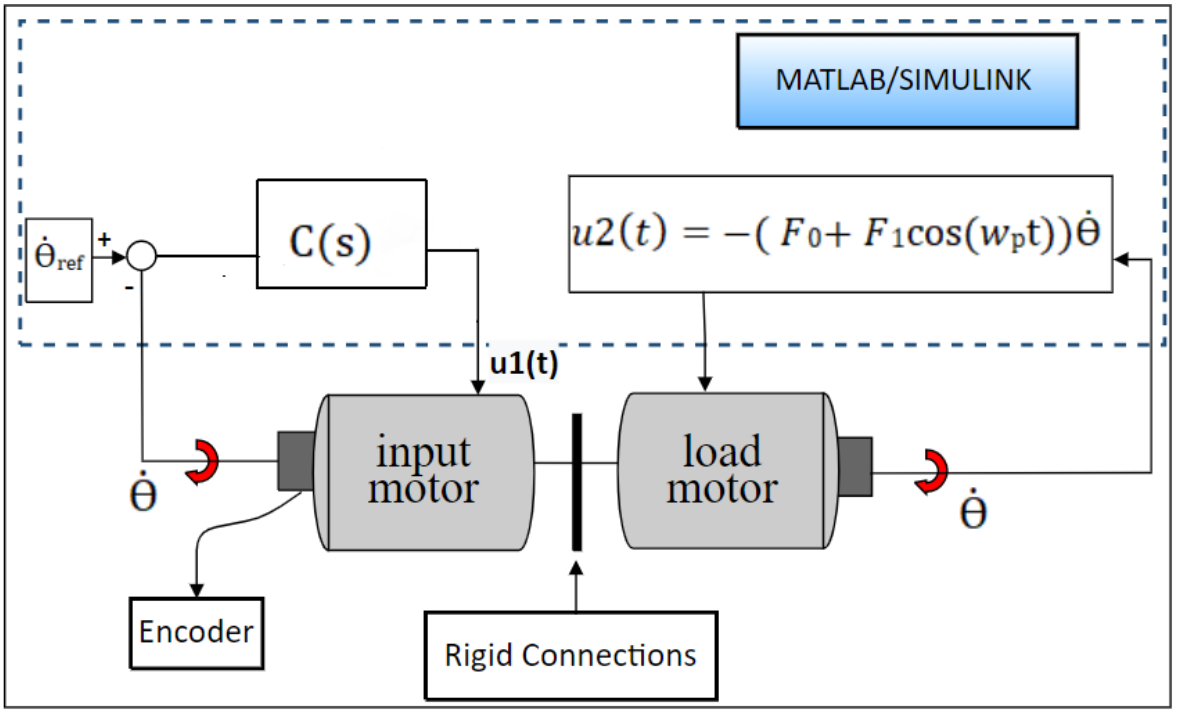

Figure 3.3 A schematic of the proposed LTP test bench. The hardware side consists of two mechanically-coupled DC motors, motor drivers, and a microcontroller. The software is implemented in Matlab/Simulink and then deployed into the microcontroller.

Controllers can be deployed to the system as in Fig. 3.3. According to the output of angular velocity $\dot{\theta}$, generated from encoder data, the controller generates commands to the plant(input motor). The controllers in this thesis are both in LTI and LTP forms.

The block diagram in Fig. 3.4 is designed to perform system identification at $100\ Hz$ loop frequency. In each cycle, motor 1 and 2 reference values are discretized, motor drive signals are generated regarding measured angular velocity in the previous cycle and transmitted to the computer, whereas another Simulink diagram receives angular velocity measurements and passes them to the Matlab workspace.

More specifically, angular velocity measurements are performed by a quadrature encoder reading block programmed in C language using the interrupt feature of the microcontroller. The encoder reading structure can be found in Fig. 3.5. The utilized encoder, HEDS-5540, has 500 CPR, which is observed by two channels with a 90-degree phase difference, so 2000 rising and falling edges emerge per rotation. During each cycle, the number of edges is accumulated by the encoder block and utilized in the next cycle. Therefore, the angular velocity measurement is achieved via a custom-built s-function block in Simulink as all the other software blocks such as PWM signal generation for DC motors and data transmission to the main computer.

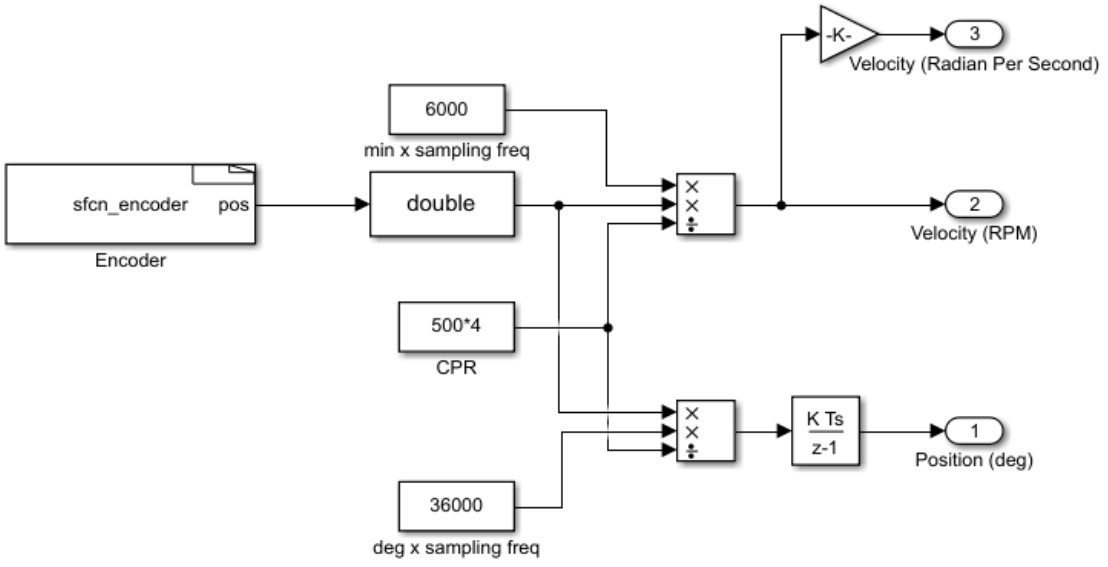

Figure 3.5 A block-diagram representation of the sensing part of the software platform. Encoder reading is performed from **sfn-encoder** block, which is an S-function block written in C language. After the necessary conversions are performed velocity and position values are obtained.

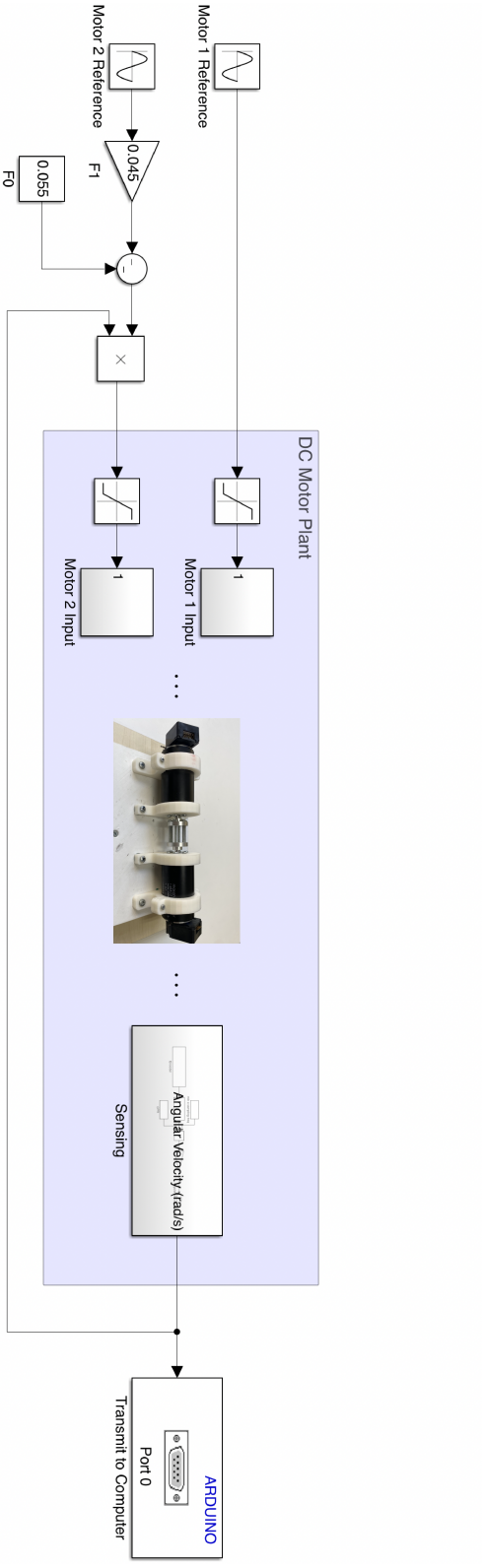

Figure 3.4 A block-diagram representation of the designed system identification software. Despite being designed in Simulink, the software is deployed to a microcontroller, working with a continuous interface with the hardware.

4. SYSTEM IDENTIFICATION of LINEAR TIME-PERIODIC SYSTEMS

At this point, we have compiled all of the necessary information to identify the frequency response functions, namely, harmonic transfer functions of linear time-periodic systems. In this chapter, we discuss the techniques for non-parametric and parametric identification of LTP systems.

Here, we conducted the system identification studies both in simulation using the Mathieu equation and in experimental setup by running actual experiments. For the Mathieu equation, we simulated its dynamics against various input signals and recorded the output measurements. Likewise, for the experimental setup, we applied various input signals to the physical LTP plant and recorded the resulting outputs.

We first adopted a non-parametric approach to estimate the harmonic transfer functions of the systems using the input–output data. These are similar to Bode plots of LTI systems and possess the ability to predict the output of the system to any input signal. However, as in the case of LTI systems, working directly with numerical frequency response functions is quite challenging during the implementation of controllers. Therefore, we employed a parametric system identification approach to estimate the unknown parameters of a state-space model of the corresponding LTP system, as outlined in [22]. Once we estimate the state-space model, it is straightforward to theoretically calculate harmonic transfer functions. We used an optimization routine during the parametric identification step to estimate the optimal system parameters that match the theoretically calculated harmonic transfer functions with the ones that are estimated based on input–output data.

4.1. Non-parametric Identification of Harmonic Transfer Functions

In previous sections, we described how to analytically derive the harmonic transfer functions (HTFs) when the state-space model of an LTP system is available. We also

explained the characteristics of the frequency response of LTP systems. The data-driven system identification methodology used in this section relies on the frequency response characteristics of LTP systems. The basic idea here is that once an LTP system is excited with a sinusoidal signal at a certain frequency, the steady-state output occurs both at the input frequency as well as the harmonics of the periodic frequency of the LTP system. Thus, a single input–output transfer function is not sufficient to represent the frequency response characteristics of LTP systems. Instead, we need to estimate multiple harmonic transfer functions to represent the overall frequency response of LTP systems.

To explain this mathematically, let the input signal be

$$u(t) = A_{in}\cos(\omega_c t + \phi_{in}), \tag{42}$$

a sinusoidal signal at frequency ω_c with amplitude A_{in} and phase ϕ_{in}. Then, the output of the LTP system at the steady state can be formulated as

$$y(t) = \sum_{n=-\infty}^{\infty} A_{out}^{n}\cos((\omega_c + n\omega_p)t + \phi_{out}^{n}). \tag{43}$$

Here, for each harmonic n, the ratio A_{out}^{n}/A_{in} defines the *gain* and the difference $\phi_{out}^{n} - \phi_{in}$ defines the *phase* of the corresponding harmonic transfer function.

For the sake of system identification, the frequency response for each HTF can be estimated as

$$\hat{H}_{\pm n}(\omega_c) = \frac{Y(\omega_c \pm n\omega_p)}{U(\omega_c)}, \tag{44}$$

where $U(\omega)$ and $Y(\omega)$ are the discrete Fourier transforms of the steady-state input and output signals, respectively.

Note that the analytically derived HTFs are in (semi)-Teoplitz form, where columns include frequency-shifted versions of the harmonic transfer functions to match the lifted input–output equation (see Fig. 4.1). Here, the estimated HTFs correspond to the middle column of the

analytically derived HTFs if a correspondence between the two representations needs to be established.

$$\hat{H}(s) = \begin{bmatrix} \vdots & \vdots & \vdots \\ \cdots \; \hat{H}_0(s - j\omega_p) & \hat{H}_{-1}(s) & \hat{H}_{-2}(s + j\omega_p) \cdots \\ \cdots \; \hat{H}_1(s - j\omega_p) & \hat{H}_0(s) & \hat{H}_{-1}(s + j\omega_p) \cdots \\ \cdots \; \hat{H}_2(s - j\omega_p) & \hat{H}_1(s) & \hat{H}_0(s + j\omega_p) \cdots \\ \vdots & \vdots & \vdots \end{bmatrix}$$

Figure 4.1 The relation between estimated HTFs and analytically derived HTFs

As mentioned earlier, the estimated harmonic transfer functions, $\hat{H}_{\pm n}$, can be used to predict the output of the LTP system for any input signal. The output of an LTP system at a certain frequency can be calculated using

$$\begin{aligned} Y(j\omega) \approx \hat{Y}(j\omega) &= \hat{H}_0(j\omega)U(j\omega) \\ &+ \hat{H}_1(j\omega)U(j\omega - j\omega_p) \\ &+ \hat{H}_{-1}(j\omega)U(j\omega + j\omega_p) \; , \end{aligned} \tag{45}$$

where the steady-state output $y(t)$ can be calculated using inverse DFT operation.

4.2. Parametric (Model-Based) Identification of LTP Systems

In this section, we treat the LTP system as a grey-box model thanks to the underlying state-space model of the target LTP system. Our goal is to estimate the unknown system parameters in the state-space model to match the frequency responses of the actual system and the state-space model. To achieve this, we estimate the optimal system parameters that yield minimum root mean squared error between the theoretically computed HTFs (based on

predicted system parameters) and the estimated HTFs that are obtained from the collected input-output data.

Let unknown state-space matrices be in the following form

$$\begin{aligned} A(t) &= \begin{bmatrix} 0 & 1 \\ -(1+\alpha cos(w_p t)) & 2\beta\zeta \end{bmatrix} \\ B(t) &= \begin{bmatrix} 0 \\ \gamma \end{bmatrix} \\ C(t) &= \begin{bmatrix} 1 & 0 \end{bmatrix} \\ D(t) &= 0 \end{aligned} \tag{46}$$

Let **p** be a vector of unknown system parameters as defined below

$$\mathbf{p} := \begin{bmatrix} \alpha, \gamma, \beta, \zeta \end{bmatrix}. \tag{47}$$

Given any numerical instantiation of **p**, we can calculate the harmonic transfer functions using analytical derivations. Let $\hat{H}_i^p$ be the i^{th} harmonic transfer function for a given **p** instantiation. Then, the parametric system identification problem is defined as

$$\mathbf{p}^* = \arg\min_{\mathbf{p}} \sum_{i=-\infty}^{\infty} |||H_i^p| - |\hat{H}_i|||_2 \tag{48}$$

There are two issues that need to be discussed here. First of all, Eq. (48) includes an infinite number of terms, which is impossible to deal with in practice. Practically, the number of harmonic transfer functions is truncated after a certain finite number. Second, the optimization problem defined in Eq. (48) is non-convex, making it impossible to use simple optimization routines. To remedy this, we used particle swarm optimization (PSO) to generate high-quality solutions with consistent convergence. Since the parametric identification procedure is completely offline, the computational load of PSO is feasible when the reward of estimating better parameters is considered. In addition, PSO is less affected by

initial conditions as compared to other alternatives, making it a robust choice for convergence algorithms. The algorithm for PSO can be found below. To avoid potential local minima issues, we perturbed the estimated parameter set around given solutions and used Matlab's "goodnessofFit" function to choose among different possible solutions.

Algorithm 1 Particle Swarm Optimization

```
Setting up the upper and lower bounds of unknown parameters of p
Initialize the particle's Theoretical HTFs with a random vector: p ∈ U(lb, ub)
Load the HTFs results from input-output data
Set the iteration number of PSO algorithm
functionPSO-Motor-Parameter-Estimation(population-size,max-
iterations,measured-transfer-function, theoretical-transfer-function)
# Initialize population of particles with random positions and velocities
particles = initialize-particles(population-size)
personal-best-positions = particles.position # initialize personal best positions
global-best-position = particles.position[0] # initialize global best position
i = 0
while i < max-iterations: do
    # Evaluate fitness of current positions
    fitness = evaluate-fitness(particles.position, measured-transfer-function,
theoretical-transfer-function)
    # Update personal best positions
    for j in range(population-size):
    If fitness[j] > evaluate-fitness(personal-best-positions[j], measured-transfer-
function, theoretical-transfer-function):
    personal-best-positions[j] = particles.position[j]
    # Update global best position
    for j in range(population-size):
    If fitness[j] > evaluate-fitness(global-best-position, measured-transfer-function,
theoretical-transfer-function)
    global-best-position = particles.position[j]
    # Update velocities and positions
    for j in range(population-size):
    particles.velocity[j] = update-velocity(particles.velocity[j], personal-best-
positions[j], global-best-position)
    particles.position[j] = update-position(particles.position[j], particles.velocity[j])
    i += 1
    return global-best-position
```

4.3. System Identification Results for the Mathieu Equation

For the simulation example of the Mathieu equation, the system matrices are chosen as

$$A(t) = \begin{bmatrix} 0 & 1 \\ -(5 - 4\cos(w_p t) & -2\zeta \end{bmatrix} \tag{49}$$

$$B = \begin{bmatrix} 0 \\ 1 \end{bmatrix}, C = \begin{bmatrix} 1 & 0 \end{bmatrix} \tag{50}$$

where $\zeta = 0.2$ and system periodic frequency $w_p = 2\pi$ rad/sec. Both theoretical and non-parametric methods were used for the analysis of the Mathieu system, which was simulated in MATLAB/Simulink environment. In the non-parametric system identification process, cosine input signals ranging from $0.1\ Hz$ to $15\ Hz$, by excluding the integer multiples of periodic frequency ($\omega_p/2 = \pi\ rad/sec$), to prevent the overlap of harmonic responses, were used. Each experiment takes 200 seconds and the data is sampled at $10\ Hz$. We used the second half of each experiment as the steady-state input–output data from the simulation output results. The HTFs were estimated using the procedures described in Sec. 4.1., taking into account the state-space matrices of the system and considering three major harmonics for calculations. First, the data-driven estimation was performed from the input–output data which was obtained from the MATLAB/Simulink simulation results. Furthermore, as we had a known state-space of the Mathieu equation, the theoretical derivation of HTFs began by transforming all the system matrices into Toeplitz structure, for detailed information see Sec. 2.3. The HTFs were then obtained by applying the Toeplitz form system matrices into the Eq. (26) and calculating the Harmonic Transfer Functions. The resulting estimated and theoretically-estimated HTFs were then plotted in Fig. 4.3..

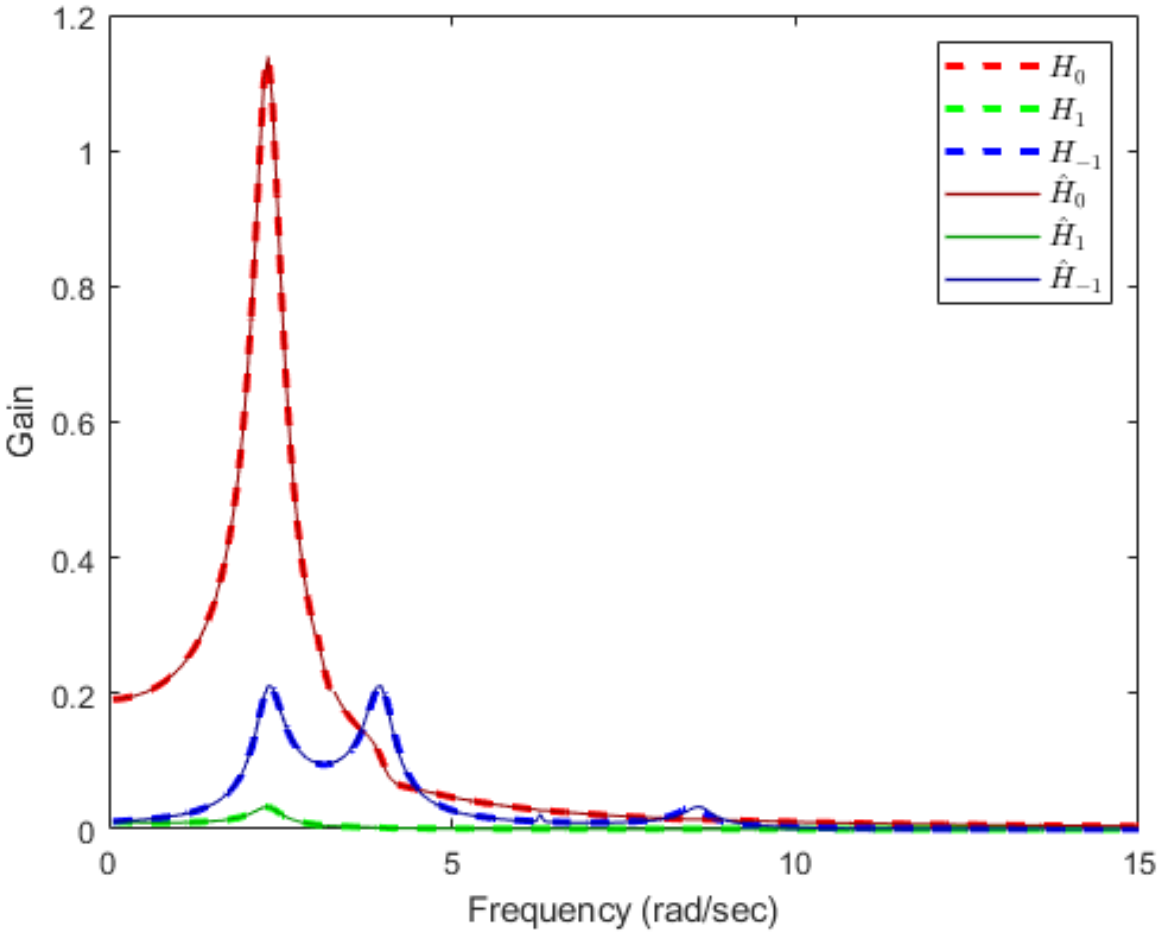

Figure 4.2 Harmonic transfer functions of the Mathieu equation. Dashed and solid lines correspond to non-parametric identification results$(\hat{H}_{\pm n})$ and theoretically calculated HTFs$(H_{\pm n})$, respectively.

We observed negligible errors in magnitude plots of estimated $(\hat{H}_{\pm n})$ and theoretically calculated HTFs $(H_{\pm n})$, where $n = -1, 0, 1$. The graph in Fig .4.3. demonstrates that each of the approaches employed for estimating the fundamental and high-dimensional, the first harmonic of the HTFs, transfer functions (HTFs) of a Mathieu equation performs effectively.

In order to demonstrate the effectiveness of the data-driven estimated high-dimensional transfer functions (HTFs), we conducted an output prediction task.

$$y(j\omega) = \sum_{n=-1}^{1} \hat{H}_{\pm n}(j\omega)U(j\omega - jn\omega_p) \tag{51}$$

Specifically, we utilized these estimated HTFs to predict the system output in response to a cosine input signal $u(t) = 0.2\cos(2.4\pi t)$ by using Eq. (51) and after that by taking the inverse Fourier Transform.

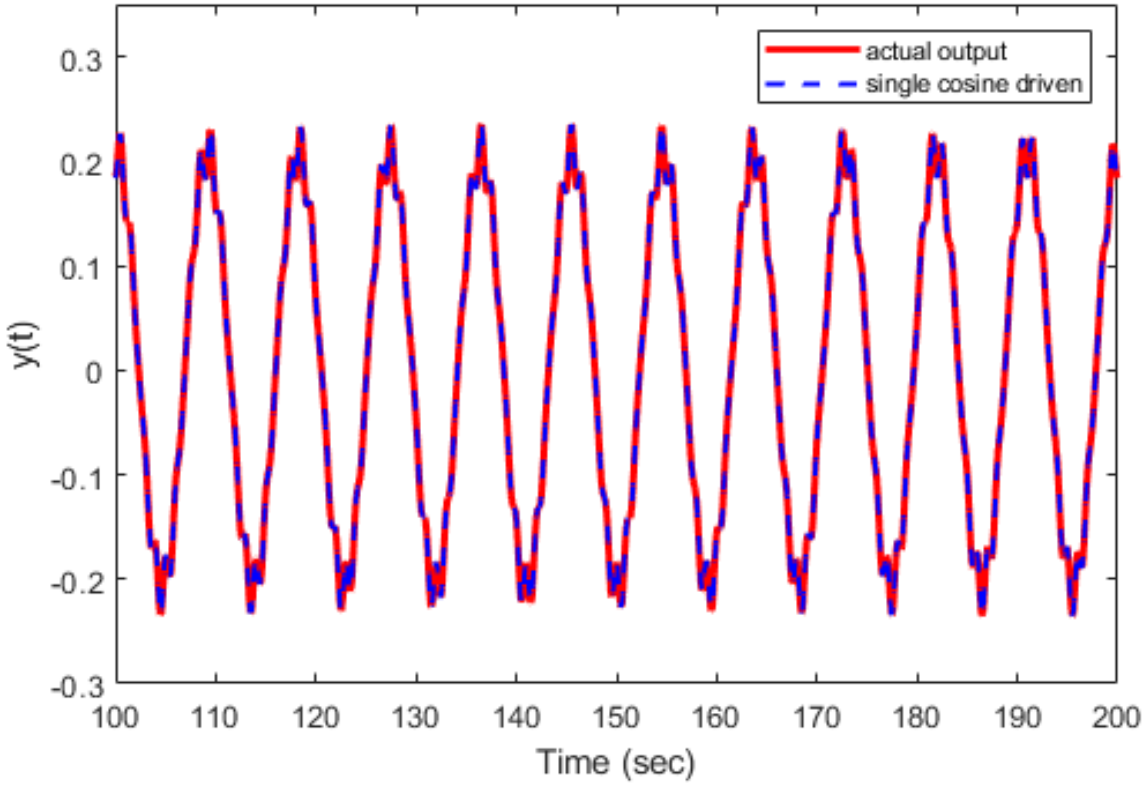

Figure 4.3 Output prediction of the Mathieu equation via estimated (Data-Driven) HTFs. The red signal is the simulation results and The blue dot signal is the output prediction of the Mathieu equation via estimated HTFs ($\hat{H}_{\pm n}$).

Fig. 4.3 shows a comparison between the actual output and the estimated output of the system. This comparison evaluates the prediction performance of the estimated harmonic transfer functions using both theoretical calculations and data-driven identification methods. The results demonstrate the ability of these methods to accurately estimate the behavior of the system. The dashed red, blue, and green lines correspond to theoretically found H_0, H_{-1}, H_1, The solid red, blue, and green lines correspond to data-driven estimated $\hat{H}_0$, $\hat{H}_{-1}$, $\hat{H}_1$, respectively within the range of system identification. The HTFs can successfully predict the output of the actual system at the steady state.

4.4. LTP Experimental Test Bench Identification Results

In the first part of this section, we approached the physical LTP test system in a black-box model by utilizing non-parametric (data-driven) system identification methods as previously discussed. We then calculated the harmonic transfer functions using these methods and subsequently compared them to those obtained through parametric identification techniques.

4.4.1. Data-Driven System Identification of the Experimental Test Bench

In the initial analysis of the system, the open loop poles were determined by computing the eigenvalues of the matrix $\mathcal{A} - \mathcal{N}$ in the fundamental region. The calculated poles were found to be $s1 = -34.4385$ and $s2 = -76.3910$. As there were no poles in the right half plane, it can be inferred that the system is stable. Based on this stability, the previously discussed non-parametric system identification technique was applied to the position and velocity control of an experimental test bench with two DC motors that were connected by a rigid connection (Fig. 3.2). It is significant to highlight that there was no prior knowledge available regarding the state-space model of the experimental test platform. We only had knowledge about the input signal and their related output signals. In our experiments, we worked with sinusoidal input signals ranging from $0.1\ Hz$ to $9.9\ Hz$, yielding a total of 89 experiments, excluding the integer multiples of periodic frequency ($\omega_p/2 = 1\ Hz$). Each experiment took 20 seconds and the data was sampled at $100\ Hz$. We used the second half of each experiment as the steady-state input–output data. We then estimated the HTFs using the procedures described in Sec. 4.1.. Note that in a practical setting, it is not possible and there is no need to calculate the possibly infinite number of HTFs. Instead, we decided the number of harmonics by observing the frequency response data that was given in Fig. 4.4 results. Here, we estimated three harmonic transfer functions, since the periodic nature of the test bench only yields first-order harmonics in the output response.

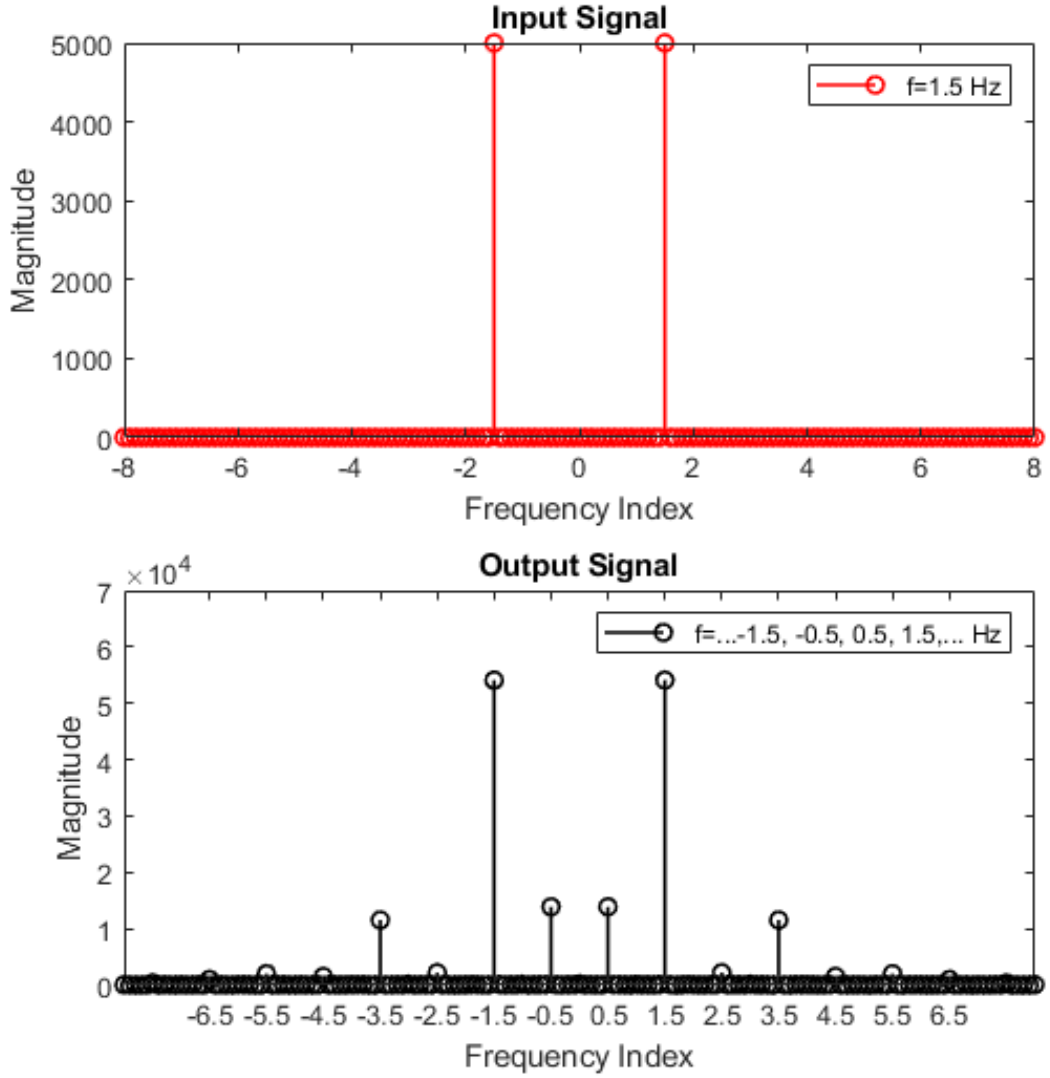

Figure 4.4 FFT plot of given input signal in a specific frequency and the FFT response of experimental test platform with 2 Hz natural periodic frequency and result from that property, periodic impulses in -1.5, -0.5, 0.5, 1.5Hz.

4.4.2. Parametric Identification of a State-Space Model for the Experimental Test Bench

Eq. (40) describes a grey-box parametric state-space model for the LTP system test bench with some unknown system parameters, K, T_m, J, and B_m. We tried to identify the unknown parameters for obtaining a state-space model for the LTP test bench. To achieve this process we used equation Eq. (48) and identify the optimal system parameters that yield minimum root mean squared error between the theoretically computed HTFs and the estimated HTFs.

Let **p** be a vector of unknown system parameters as defined below

$$\mathbf{p} := \Big[K, T_m, J, B_m\Big]. \tag{52}$$

Given any numerical instantiation of **p**, we can calculate the harmonic transfer functions using analytical derivations. Let $\hat{H}_i^p$ be the i^{th} harmonic transfer function for a given **p**. Then, the parametric system identification problem can be performed as in Eq. (48).

This optimization routine yielded the optimal plant parameters that match the HTFs calculated by the state-space model with the HTFs estimated directly from the input–output data. Fig. 4.5 and 4.6 illustrate the resulting HTFs calculated with the optimal system parameters. Note that the computed HTFs are smoother as compared to the data-driven estimations and their characteristics match the estimations. Table 4.1 lists the parameters estimated from the optimization routine. We used the procedure and algorithm that is described in Sec. 4.2.

Table 4.1 Estimated motor parameters

$J\ (kg\,m^2)$	$T_m\ (s)$	$B_m\ (Nm\,s\,/\,rd)$	$K\ (Nm\,/\,V)$
0.0098	0.0056	0.1268	2.9142

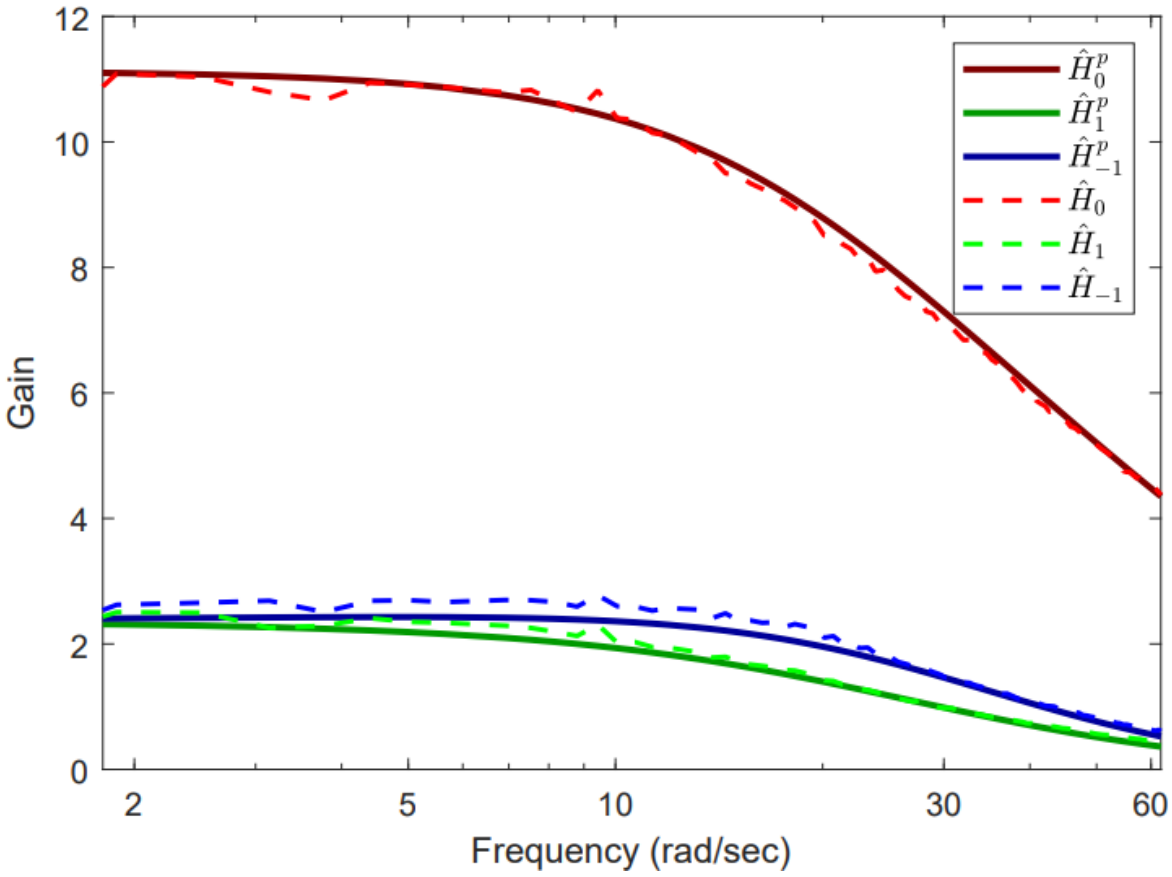

Figure 4.5 Harmonic transfer functions of the LTP system test bench. The HTF prediction is calculated via the velocity output of the system. Dashed and solid lines correspond to non-parametric and parametric identification results which are the relationships between the input and the velocity output of the system, respectively.

Fig. 4.5 and Fig. 4.6 illustrate estimated harmonic transfer functions. The dashed red, blue, and green lines correspond to $\hat{H}_0$, $\hat{H}_1$, and $\hat{H}_{-1}$, respectively within the range of system identification. The estimation of HTFs was performed both via angular velocity and angular position input-output data.

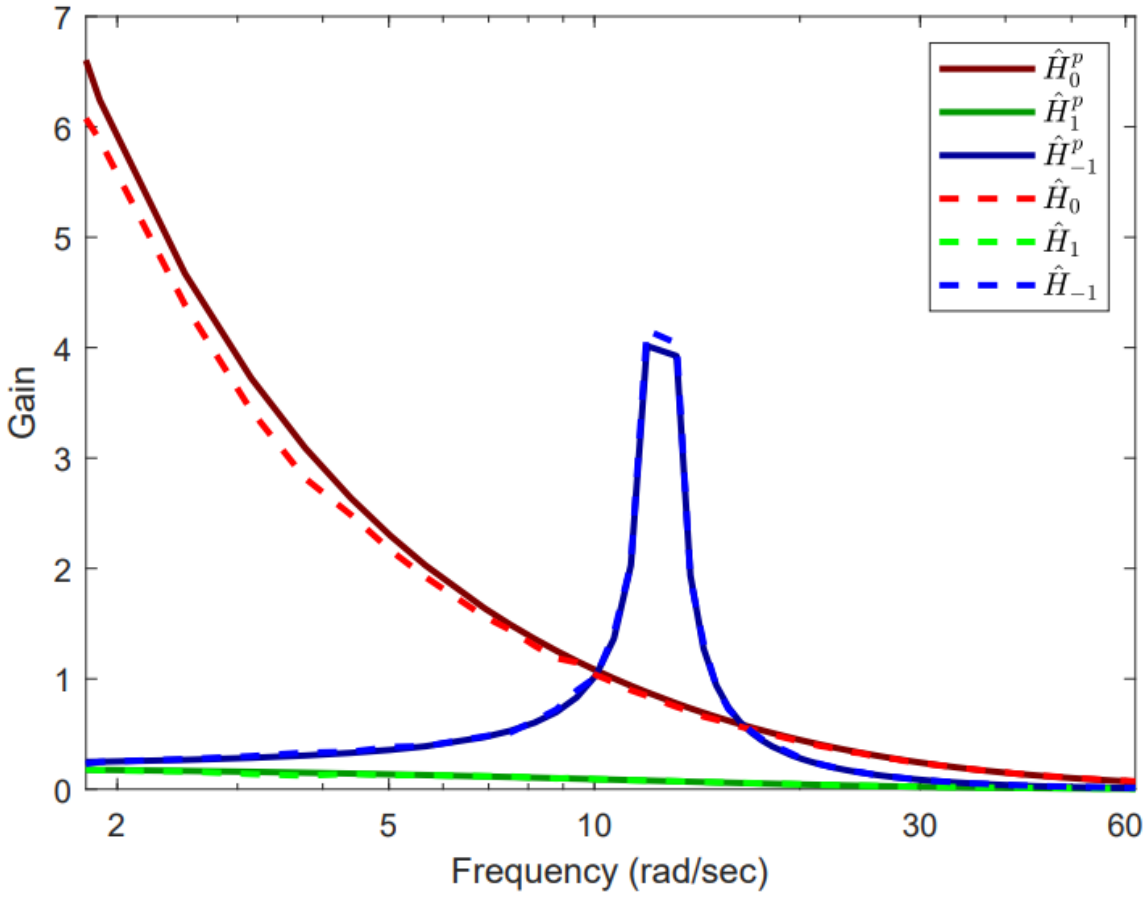

Figure 4.6 Harmonic transfer functions of the LTP system test bench. The HTF prediction is calculated via the position output of the system. Dashed and solid lines correspond to non-parametric and parametric identification results which is the relationship between input and the position output of the system, respectively.

We assessed the prediction performance of the HTFs using a test signal, that was previously used during the system identification procedure. Fig. 4.7 illustrates the LTP test bench's steady-state response, only half of the output data were used for analyses (Input–Output data between 10-20 seconds), and the system's predicted output was obtained using the estimated HTFs. First, one can quickly notice the multi-frequency content of the output signal to a constant-frequency sinusoidal at the input. The HTFs can successfully predict the output of the actual test bench at the steady state. We also calculated the error values based on the difference between the predicted and experimentally obtained system responses to the specific input signals :

$$E_{rms} := \frac{\sqrt{\frac{1}{T}(\sum_0^T (y(t) - \hat{y}(t))^2)}}{\sqrt{\frac{1}{T}(\sum_0^T y(t)^2)}} \tag{53}$$

Where T is the duration of the steady-state value of the input sinusoidal signal. The related E_{rms} values for different frequency input signals can be found in Tab. 4.2.

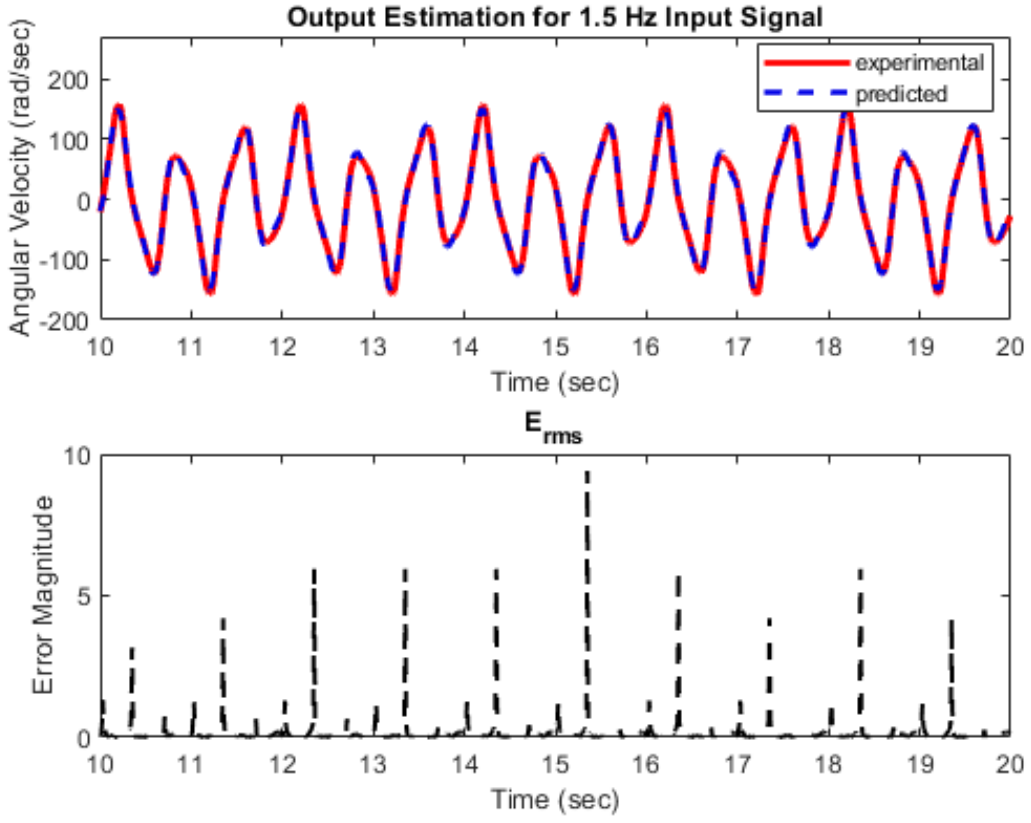

Figure 4.7 Prediction performance of the HTFs in the time domain for an excitation input at $1.5\ Hz$. The first graph is the output prediction for an excitation input at $1.5\ \ Hz$. The second graph is the E_{rms} values between the predicted and the experimental system response

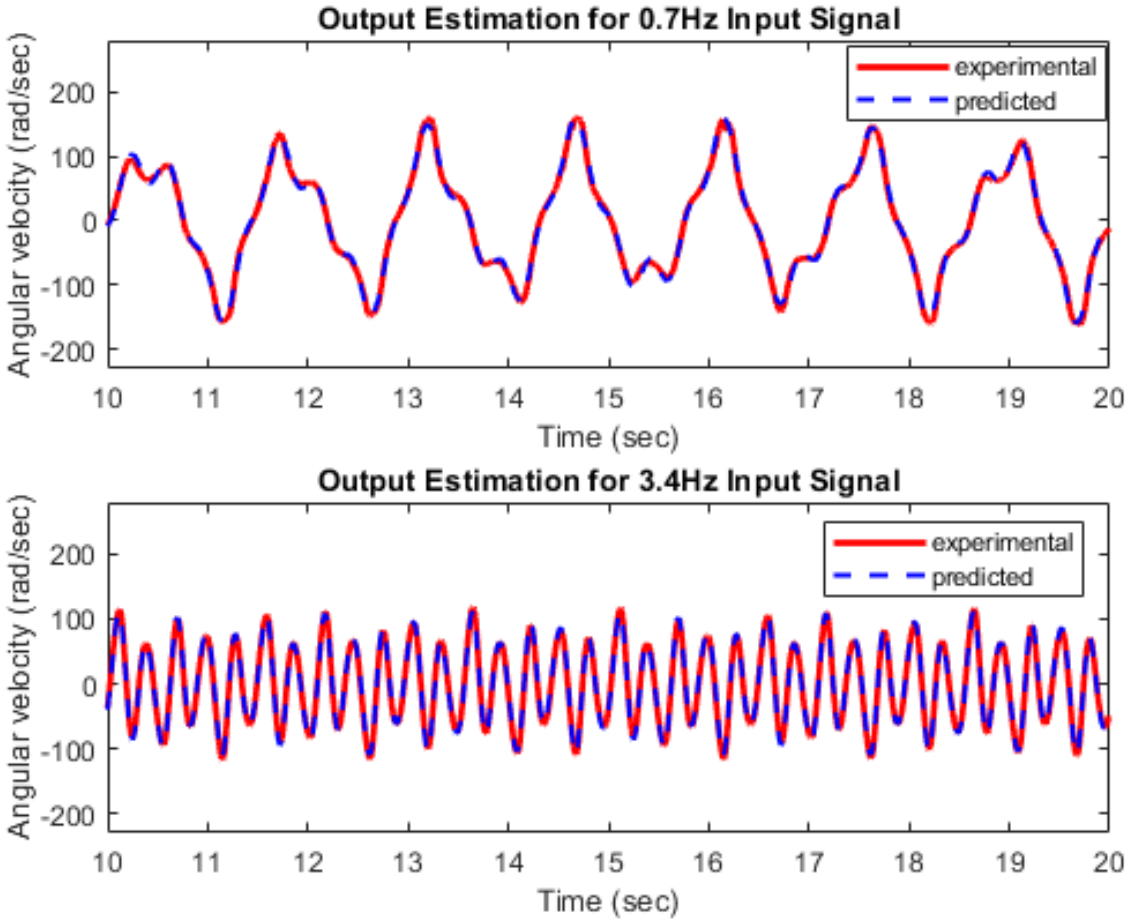

Figure 4.8 Prediction performance of the HTFs in the time domain for an excitation input at in turn 0.7 Hz and 3.4 Hz .

Table 4.2 E_{rms} values for output estimation with different frequency input signals

	0.7 Hz	1.5 Hz	3.4 Hz
E_{rms}	0.0622	0.0625	0.0606

5. CONTROLLER DESIGN FOR LINEAR TIME-PERIODIC (LTP) SYSTEMS

There are some previous works that focus on designing LTI controllers for LTP systems using harmonic transfer functions and lifted LTI representations of the actual time-periodic dynamics [16, 25, 38]. Different than these works, in this part we utilized the parametrically identified state-space model for controller design. Besides, the key difference in our work was the experimental validation of the LTI and LTP controllers on a physical LTP system plant unlike the previous work, which was only tested in simulation [25]. We first validated our results in simulation both on the Mathieu equation and the state-space model of the test bench. Then, we transferred and tested the controllers on the actual physical platform.

5.1. Time-Periodic Linear Optimal Quadratic Regulator (LQR) Controller Design for LTP Systems

The LQR controllers are one of the preferred controller types for the LTP systems [39–41], especially for the helicopter vibration control [26, 27, 42] and also several application examples for DC motor systems [43, 44]. The key reason behind the successful application of LQR methods on LTP systems is our ability to lift the LTP state-space models to a higher dimensional LTI form. This greatly simplifies the design of LQR controllers for LTP systems, since technically the plant is transformed into an LTI form. Note that the LQR gains in this methodology are also calculated in the lifted LTI form.

This section presents an overview of the LQR controller design basics and establishes the terminology used throughout the section. We explained a method for controller design based on a Ricatti-based solution for LTP systems. To demonstrate the effectiveness of this method, various examples were provided and analyzed to compare the performance of LQR controllers.

5.1.1. Linear Quadratic Regulator

The LQR control method is used to improve the stability and robustness of closed-loop systems by using feedback gains. This involves solving the Matrix-Riccati differential equation, which requires a thorough understanding of the system's state-space model. However, implementing LQR control can be difficult when only the harmonic transfer functions are available and the state-space model of a Linear Time-Periodic (LTP) system is unknown.

Consider the known LTP system state-space model of the form

$$\dot{x}(t) = A(t)x(t) + B(t)u(t) \tag{54}$$

with the classical assumption that $A(t)$ and $B(t)$ are T -periodic matrices, with zero initial state conditions.

The primary objective of the Linear Quadratic Regulator (LQR) problem is to develop a full-state feedback control law, which uses the current state of the system to determine the control input.

The law is,

$$u(t) = -K_{LQR}(t)x(t) \tag{55}$$

that minimizes the quadratic cost function. Where $K_{LQR}(t)$ is the time-periodic state feedback gain.

The quadratic cost function is

$$J(0, t_f) = \int_0^{t_f} (x^T(t)Q(t)x(t) + u^T(t)R(t)u(t))dt + (x^T(t_f)P_f x(t_f)) \tag{56}$$

where $R(t)$ penalizes the control input and R(t) is uniformly positive definite, T -periodic, symmetric matrix for all $t \in [0, T]$. $Q(t)$ provides weighting for the system states. P_f is the positive definite, constant, and symmetric matrice. The Q and R matrices in the

Linear Quadratic Regulator (LQR) problem are used to balance the trade-off between the performance and control effort, respectively.

The optimal full state feedback gain $K_{LQR}(t)$, which guarantees that the closed-loop stability is calculated by

$$K_{LQR}(t) = R^{-1}(t)B^T(t)P(t) \tag{57}$$

The symmetric non-negative definite matrix $P(t)$ satisfies the Control Matrix Riccati Differential Equation (CMRDE):

$$-\dot{P}(t) = P(t)A(t) + A^T(t)P(t) + Q(t) - P(t)B(t)R^{-1}(t)B^T(t)P(t)\ . \tag{58}$$

with terminal condition

$$P(t_f) = P_f. \tag{59}$$

When the termination time $t_f \to \infty$, $P(t)$ approaches the steady state value independent from the P_f. The optimal solution of the cost function is given by

$$J(t, t_f) = x^T(t)P(t)x(t)\ . \tag{60}$$

Please see [16, 45] for further details.

In earlier sections, the concept of using the harmonic balance approach was presented for linear time-periodic (LTP) systems. This section continues with the discussion of applying the harmonic balance methodology to the Control Matrix Riccati Differential Equation (CMRDE). It should be noted that the application of the Toeplitz transforms to the Riccati Differential Equation (RDE) results in infinite-dimensional algebraic Riccati equations.

At the steady state, $P(t)$ is time-periodic with period T or $P(t+T) = P(t)$. The remaining matrices are also periodic with period T. Harmonic balance method analysis starts with taking the Toeplitz transform of Eq. (58). Since we take the Toeplitz transform of A matrix, that will be replaced with $A - N$. If we have periodic coefficients in the B matrix, we also

deal with it.

$$0 = P(A - N) + (A - N)^T P + Q - PBR^{-1}B^T P \tag{61}$$

This equation is called the Control Matrix Riccati Harmonic Balance Equation (CMRHBE). For further information, please see [16].

5.1.2. Solution of the CMRHBEs

Various strategies are described for solving periodic Algebraic Ricatti Equation (ARE) [33]. To tackle the infinite-dimensional structure of the Control Matrix Riccati Harmonic Balance Equation (CMRHBE), the matrices must be truncated to a finite dimension for computational needs. This results in a complex algebraic Riccati equation (ARE), which can be solved by conventional methods such as MATLAB, or by using the procedure proposed in this thesis, specifically for Toeplitz systems. The solvers for ARE are robust in handling complex arithmetic and therefore can be used instead of the method described here. The augmented system matrices (A, B, C, D, N) and the weight matrices (Q, R) are redefined in a specific form to facilitate the solution process as

$$A_1 = \begin{bmatrix} Re(A) & Im(A) \\ -Im(A) & Re(A) \end{bmatrix} \tag{62}$$

$$B_1 = \begin{bmatrix} Re(A) & Im(B) \\ -Im(B) & Re(B) \end{bmatrix} \tag{63}$$

and also the weights matrices Q_1 and R_1 are has the same structure. Also $Re(N) = 0$, so

$$N_1 = \begin{bmatrix} 0 & Im(N) \\ -Im(N) & 0 \end{bmatrix} \tag{64}$$

The augmented system and weight matrices can be expressed using real numbers by applying a similarity transformation, which preserves the eigenvalues and eigenvectors of the matrices.

This concept can be demonstrated through the use of the following similarity transformation matrix.

Let T_1 be

$$T_1 = \frac{1}{\sqrt{2}} \begin{bmatrix} I & I \\ jI & -jI \end{bmatrix} . \tag{65}$$

It holds to property of $T_1^{-1} = T_1^*$ and also

$$\begin{bmatrix} A & 0 \\ 0 & A \end{bmatrix} = T_1^* A_1 T_1 \tag{66}$$

The Ricatti equation in Eq. (67) is a real-valued infinite dimension Ricatti equation as

$$0 = P_1(A_1 - N_1) + (A_1 - N_1)^T P_1 + Q_1 - P_1 B_1 R_1^{-1} B_1^T P_1 . \tag{67}$$

After truncating the number of harmonics to N, the problem is reduced to solving a set of $(2N+1)n$ equations, with n being the same dimension of matrix A. By solving the Algebraic Riccati Equation, the Fourier Sine or Cosine coefficients of the Trigonometric Fourier series expansion of the time-periodic LQR feedback gains are derived. The center block row of the Toeplitz form matrix can be used to obtain the periodic LQR gain matrix, and further time-domain calculations can be performed via the method explained below.

For example, assume that the center block row of the K_{LQR} matrix in the following form,

$$K_{LQR} = \begin{bmatrix} a + bi & 0 + 0i \\ x + 0i & y + 0i \\ a - bi & 0 - 0i \end{bmatrix} . \tag{68}$$

The complex number $(a + bi)$ can be represented as

$$\begin{aligned} r &= abs(a + bi) \\ \omega &= angle(a + bi) \\ z &= re^{(i\omega)} \end{aligned} \tag{69}$$

And after that conversion is performed, the sum of these signals can be written as a cosine function

$$\cos(\phi t) = \frac{e^{(i\phi t)} + e^{(-i\phi t)}}{2} \ .$$

By performing the inverse Fourier series transform, with the help of Euler formulas, periodic K_{LQR} can be obtained.

To address the regularization problem, the Linear Quadratic Regulator (LQR) state feedback gains can be implemented. Additionally, in order to ensure tracking, two different control structures are used in this thesis. The first one combines the precompensator gain with the periodic LQR gain matrix, while the second one is based on the design of a Linear Quadratic Integrator (LQI). These control structures work in conjunction to achieve the desired level of performance and control effort.

5.1.3. LQR Design with Precompensator Gain

A precompensator has been integrated into the system in order to reduce the steady-state error to an insignificant value and enhance the reference tracking performance. The related formula for precompensator gain g is as

$$\frac{1}{g} = C(BK_{LQR} - A)^{-1}B \ . \tag{70}$$

The same procedure that is described in Sec. (5.1.2.) for K_{LQR} calculations was used for designing the precompensator gain g. For constant g calculations the $(A0, B0, C0, D0)$ matrices are used. For time-varying precompensator gain g calculations the system matrices

(A, B, C, D) are used with the help of the formula in Eq. (70). By taking the center block row of that Teoplitz form matrix, precompensator gain can be obtained. In this thesis, we performed analysis both with LTI-type and LTP-type precompensator gains. The LQR-based controller structure with precompensator gain is given in Fig .5.1. And the control signal becomes

$$u(t) = -K_{LQR}(t)x(t) + g(t)u_{ref} \ . \tag{71}$$

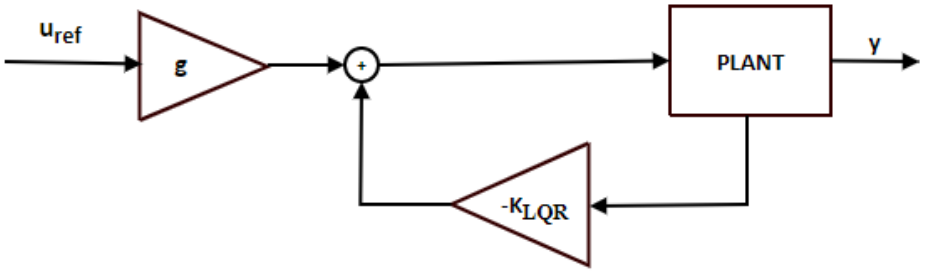

Figure 5.1 The reference tracker state feedback time periodic LQR design structure with additional precompensator gain

5.1.4. Linear Quadratic Integrator (LQI) Design

The LQI controller is a type of feedback control strategy that is designed to address the issue of steady-state error that arises in linear time-periodic (LTP) systems. In such systems, the output may have a periodic component that remains non-zero even when the system is under control, leading to a steady-state error. The LQI controller aims to eliminate this issue by adding an integral term to the feedback control that integrates the error over time and adds it to the control input to compensate for the periodic component of the output. This integral term is designed to continuously adjust the control input, allowing the controller to effectively reduce the steady-state error in the LTP system.

The LQI scheme-based controller structure is given in Fig. 5.2.

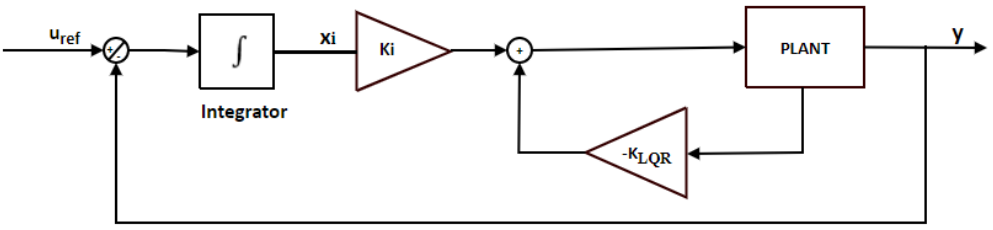

Figure 5.2 The reference tracker time-periodic LQI design structure

In order to illustrate the principles and properties of our control methodology, we started by performing our applications on the Mathieu equation and then continued with the experimental platform.

5.2. Controller Design for the Mathieu Equation in Simulation

Before starting the evaluation of the controller design, the time domain analysis of the Mathieu equation, represented in the state-space form as described in equations Eq. (49,50), is performed to understand the enhancement in performance. The time-domain open-loop step response of the Mathieu system is illustrated in Fig. 5.3.

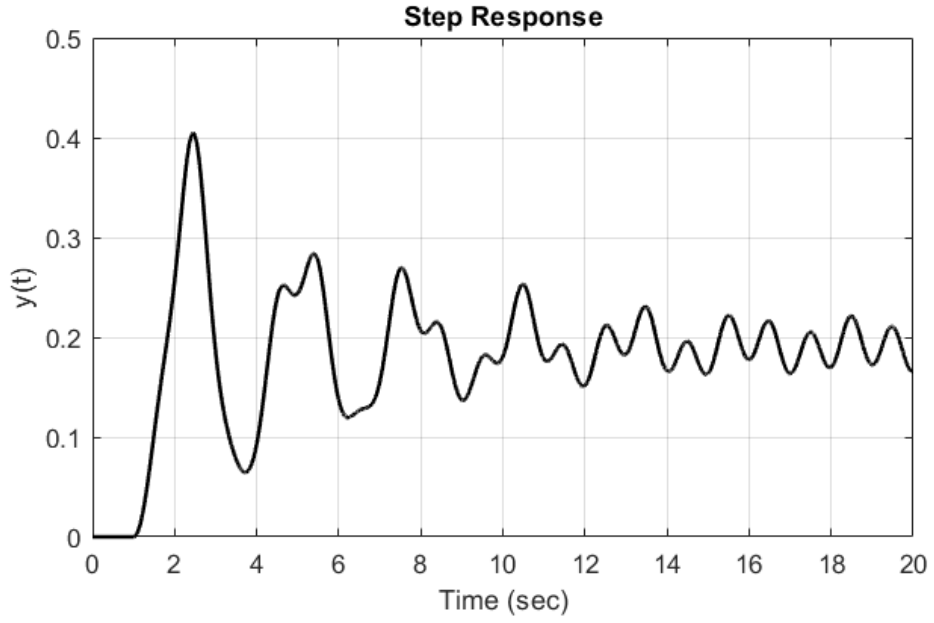

Figure 5.3 Step response of the open-loop Mathieu Equation

From the graph in Fig. 5.3, the open-loop time-domain performance of the Mathieu equation is given in Tab. 5.1.

Table 5.1 Open loop Mathieu equation time domain results

Percentage Overshoot (PO)	Settling Time (sec)	Rise Time (sec)
108	24	1.55

The open loop frequency-domain performance of the Mathieu equation results can be found in Tab. 5.2.

Table 5.2 Open loop Mathieu equation frequency domain results

Phase Margin (degree)	Delay Margin (sec)	Bandwidth (rad/sec)
32.8	0.423	1.51

In the previous works, different types of controllers, such as P, PI, PID, LQR, are designed to enhance the system performance [25] but all the controllers have LTI form and have no periodic effect. Unlike these works, we used a method for calculating the periodic LQR controller gains and also LTI-LQR controller gains for the LTP systems. Both of the results were explained in the time and frequency domain in the following sections.

5.2.1. Periodic LQR Controller Design for the Mathieu Equation in Simulation

In this section, we used the method described in Sec. 5.1.3. to investigate the effect of periodic controllers on LTP systems and give the stabilization (or regulation) and reference tracking performances. The precompensator gain is added to the closed-loop system to have better dynamics, and to improve the system's robustness, stability, and performance. For instance, it can be used to increase the system's Bandwidth, reduce the phase lag, or improve the disturbance rejection.

a. Case Study #1

A Periodic LQR controller was designed for the Mathieu equation based on the below design conditions. The weight matrices are chosen as

$$\begin{aligned} R &= 0.1 \\ Q &= \begin{bmatrix} 1 & 0 \\ 0 & 1 \end{bmatrix} \end{aligned} \tag{72}$$

with the calculated precompensator gain equal to 6.2385. The periodic LQR gain matrix K_{p-LQR} and LTI gain matrix K_{LQR} were calculated as in Eq. (73,74) and deployed to the Mathieu system in the following form:

$$K_{p-LQR} = [1.2385 + 2.2144\cos(2\pi t + 0.7682), 3.1393 + 0.47\cos(2\pi t + 1.4971)] \tag{73}$$

$$K_{LQR} = [1.2385, 3.1393] \tag{74}$$

The Bode plots of the uncontrolled open loop Mathieu system, for the fundamental harmonic (H_0), the closed loop system with LTP type K_{p-LQR} controller in Eq. (73), and the LTI type K_{LQR} controller in Eq. (74) were given in Fig. 5.4.

In Fig. 5.4, the red signal is the closed loop system with LTI-LQR controller, the black dashed signal is the LTP-LQR closed loop system and the blue is the open loop Mathieu equation. The frequency domain analysis was performed by checking the bandwidth, delay margin, and phase margin results from the Bode plot in Fig. 5.4.

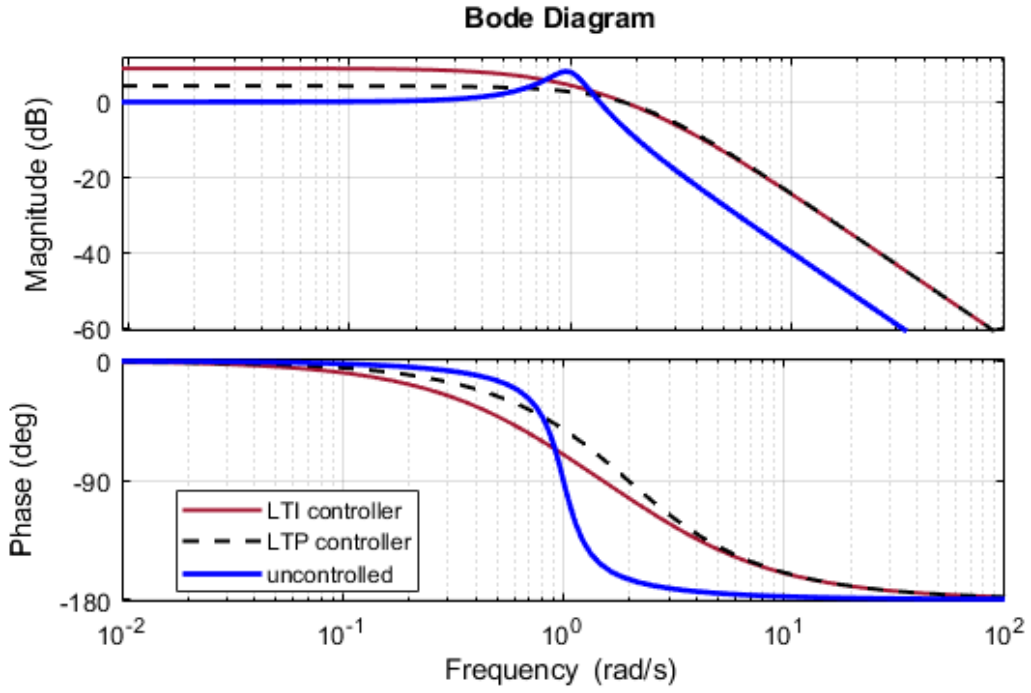

Figure 5.4 The Bode plots of the uncontrolled system, the system with LTP-LQR controller ($K_{p-LQR} = [1.2385 + 2.2144\cos(2\pi t + 0.7682), 3.1393 + 0.47\cos(2\pi t + 1.4971)]$), and the system with LTI-LQR controller ($K_{LQR} = [1.2385, 3.1393]$).

Table 5.3 Closed loop Mathieu equation frequency domain results with $K_{p-LQR} = [1.2385 + 2.2144\cos(2\pi t + 0.7682), 3.1393 + 0.47\cos(2\pi t + 1.4971)]$ and $K_{LQR} = [1.2385, 3.1393]$

Controller Type	Phase Margin (degree)	Delay Margin (sec)	Bandwidth(rad/sec)
LTI	82.5	0.824	2.31
LTP	97.7	0.986	2.40

The system without any controller has a phase margin of $32.8\ degrees$ and with the LTI-LQR controller design, it reached the value of $82.5\ degrees$ even with the LTP-LQR controllers, it reached better results $(97.7\ degrees)$. The observations are also the same for the delay margin and the bandwidth results. The delay margin of the uncontrolled system is $0.423\ sec$ and after the controllers were deployed to the system it reaches the value of $0.824\ sec$ for the LTI case and $0.986\ sec$ for the LTP case. Increasing the bandwidth of the motor system is a crucial necessity to promptly address sudden disturbances. LQR controllers have facilitated

the enhancement of the bandwidth from an initial value of $1.52\ rad/sec$ to $2.31\ rad/sec$, with detailed explanations provided in Table 5.3.

The performance of the controller in tracking the reference signal was evaluated by providing the Mathieu system to step and sinusoidal signals. The step input signal was applied to the system after $1\ sec$ as a reference signal. The reference tracking performance with the step input signal can be found in Fig. 5.5.

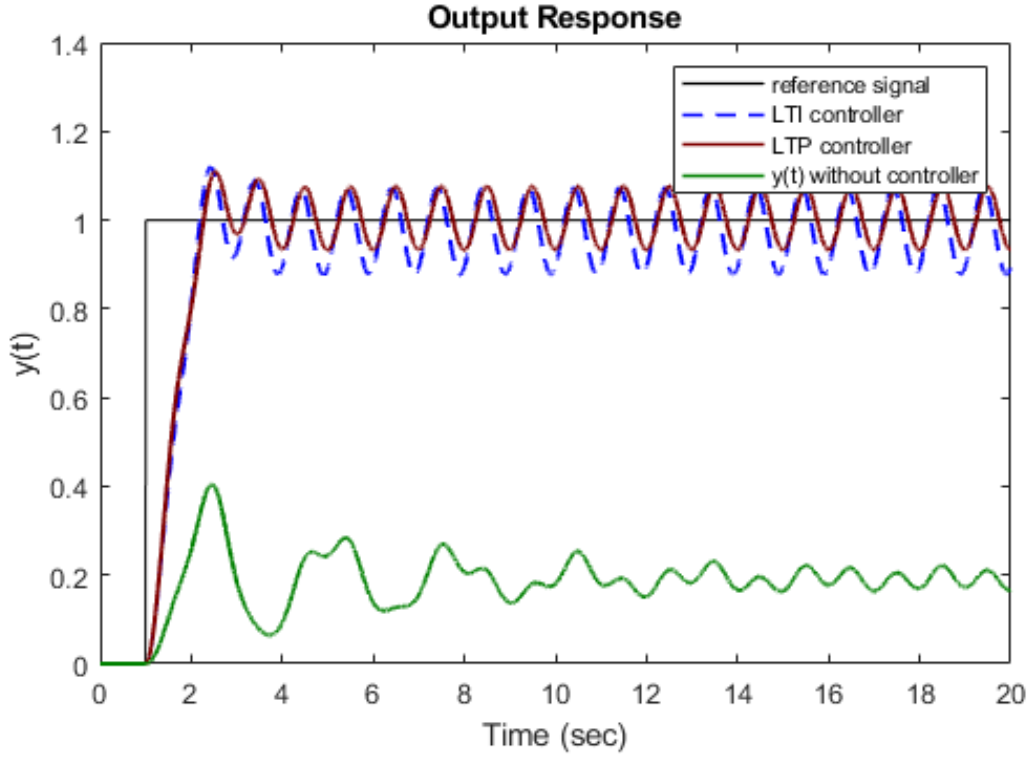

Figure 5.5 Step response of the Mathieu equation. The red signal is the step response of the precompensator LTP-LQR $K_{p-LQR} = [1.2385 + 2.2144\cos(2\pi t + 0.7682), 3.1393 + 0.47\cos(2\pi t + 1.4971)]$ and the blue signal is the step response of the precompensator LTI-LQR $K_{LQR} = [1.2385, 3.1393]$ system response. The green response is the uncontrolled system without any controller.

Table 5.4 E_{rms} values for LTI ($K_{LQR} = [1.2385, 3.1393]$) and LTP type LQR $K_{p-LQR} = [1.2385 + 2.2144\cos(2\pi t + 0.7682), 3.1393 + 0.47\cos(2\pi t + 1.4971)]$ controller

	Uncontrolled	LTI Controller	LTP Controller
E_{rms}	0.8117	0.1685	0.1575

Tab. 5.4 presents the Root Mean Square Error (RMSE) values obtained for both LTI and LTP controllers. It can be inferred that the LQR-based controllers exhibit satisfactory tracking performance. However, the RMSE values for the LTP controller are lower than those for the LTI controller, indicating that the LTP controller performs better in terms of tracking accuracy with respect to the step input signal.

The settling time of the uncontrolled system is nearly $24\ sec$, whereas the system under LQR control achieves settling times of $3.03\ sec$ and $2.94\ sec$, respectively. This highlights the efficiency of the LQR controller in reducing settling time and improving system stability.

The time-domain analysis involved a comprehensive assessment of the impact of LTI and LTP-type LQR controllers on the Percentage Overshoot (PO) and Settling Time.

Table 5.5 Closed loop Mathieu equation with $(K_{p-LQR} = [1.2385 + 2.2144\cos(2\pi t + 0.7682), 3.1393 + 0.47\cos(2\pi t + 1.4971)])$ and $(K = [1.2385, 1.4971])$ time domain results

Controller Type	Percentage Overshoot(PO)	Settling Time (sec)
LTP	4.668	3.03
LTI	6.462	2.94

The results in Tab. 5.5 show that both controller types are efficient in reducing PO, and the settling time. The LTP-type controllers exhibited an even greater reduction in PO when compared to the LTI-type. However, this reduction was accompanied by a minimal increase in settling time, as presented in Tab. 5.5.

The control inputs for the velocity state, and the position state can be found in Fig .5.6. Also in order to evaluate the ability of the system to track a sinusoidal signal, a sinusoidal input signal of the form $u_{ref}(t) = \sin(0.4t)$ was applied to the system in Fig. 5.7.

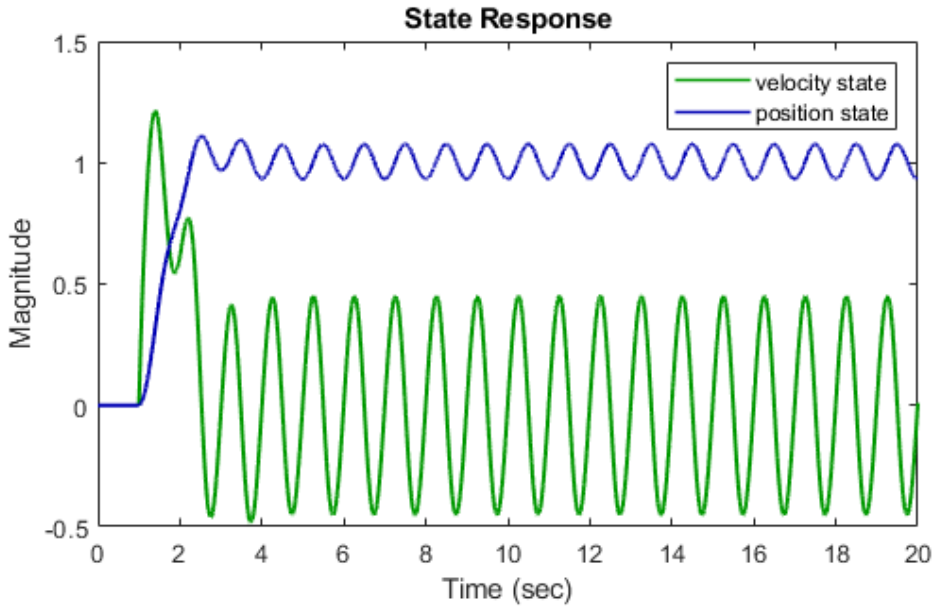

Figure 5.6 Control input signals of the closed-loop Mathieu equation with precompensator-LQR controller. The green signal is the control input for the velocity state and the blue signal is the control input for the position state.

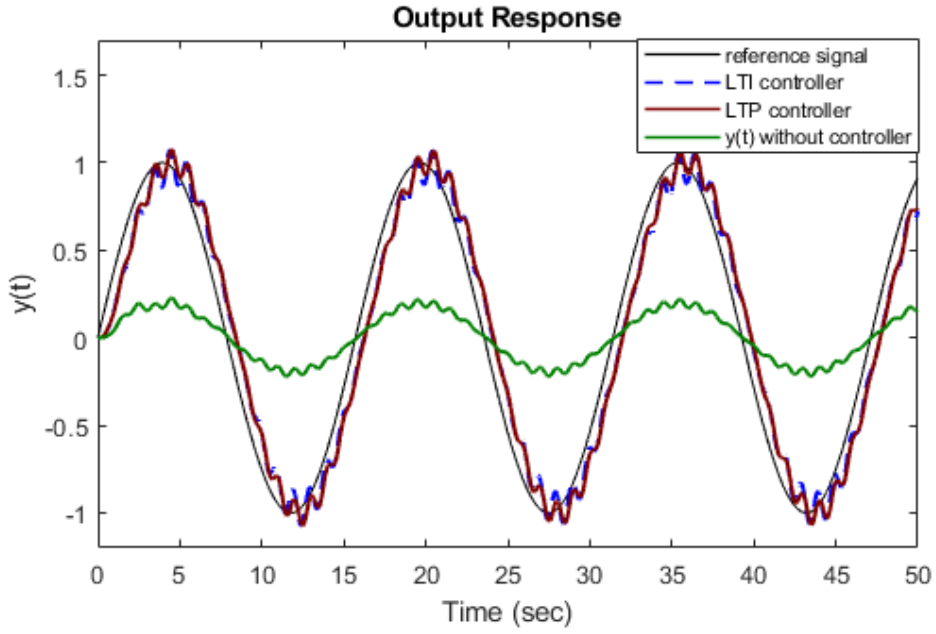

Figure 5.7 Output response of the Mathieu equation. The red signal is the response of the system with the precompensator LTP-LQR and the blue signal is the precompensator LTI-LQR system response and the green is the system response without a controller.

The corresponding results are presented in Fig. 5.7 for the Mathieu equation, both LTI and LTP type LQR controllers are capable of achieving efficient reference tracking performance for a sinusoidal input signal.

b. Case Study #2

As a second example of LQR controller design, we changed the weight matrix of the first state and performed the same analysis. The chosen weight matrices R and Q are

$$\begin{aligned} R &= 0.1 \\ Q &= \begin{bmatrix} 10 & 0 \\ 0 & 1 \end{bmatrix} \end{aligned} \tag{75}$$

with the calculated precompensator gain from the related formula equal to 11.3963. The periodic-LQR gain matrix K_{p-LQR} and LTI gain matrix K_{LQR} are calculated as in Eq. (76,77) and deployed to the system.

$$K_{p-LQR} = [6.39 + 2.9\cos(2\pi t + 0.6718), 4.3774 + 0.5086\cos(2\pi t + 1.2545)] \tag{76}$$

$$K_{LQR} = [6.39, 4.3774] \tag{77}$$

The Bode plots the uncontrolled open loop system Mathieu system, for the fundamental harmonic (H_0), the system with LTP type K_{p-LQR} controller in Eq. (76), and the LTI type K_{LQR} controller in Eq. (77) is given in Fig. 5.8.

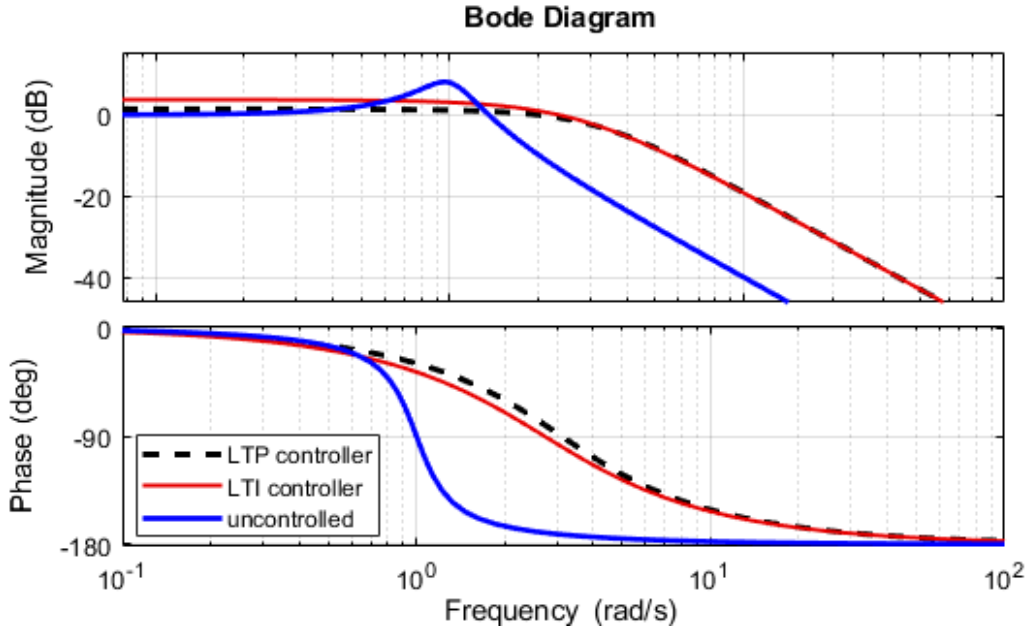

Figure 5.8 The Bode plots of the uncontrolled system, the system with LTP-LQR controller ($K_{p-LQR} = [6.39 + 2.9\cos(2\pi t + 0.6718), 4.3774 + 0.5086\cos(2\pi t + 1.2545)]$), and the system with LTI-LQR ($K = [6.39, 4.3774]$) controller.

After the calculated K_{LQR} gains are deployed to the system, the resulting delay, phase margin, and Bandwidth are obtained as in Tab 5.6.

Table 5.6 Closed loop Mathieu equation with LTP ($K_{p-LQR} = [6.39 + 2.9\cos(2\pi t + 0.6718), 4.3774 + 0.5086\cos(2\pi t + 1.2545)]$) and LTI ($K = [6.39, 4.3774]$) frequency domain results

Controller Type	Phase Margin (degree)	Delay Margin (sec)	Bandwidth (rad/sec)
LTI	99.4	0.737	3.28
LTP	120	1.04	3.25

We observe that the periodic controllers in LTP systems give better phase margin, and delay margin results, detailed information can be found in Tab. 5.6, so we may say that a system with the periodic LQR controller will be more stable and less sensitive to disturbances in that particular case.

The ability of the controller to track the reference signal is tested by providing step and sinusoidal signals. In order to analyze the tracking performance a step input was applied to the system after $t = 1\ sec$ for a duration of $20\ sec$. The related reference tracking performance results can be found in Fig. 5.9. In Fig. 5.9, the blue response represents the closed loop system with the LTI-LQR controller and the red signal is the response of the LTP-LQR controller.

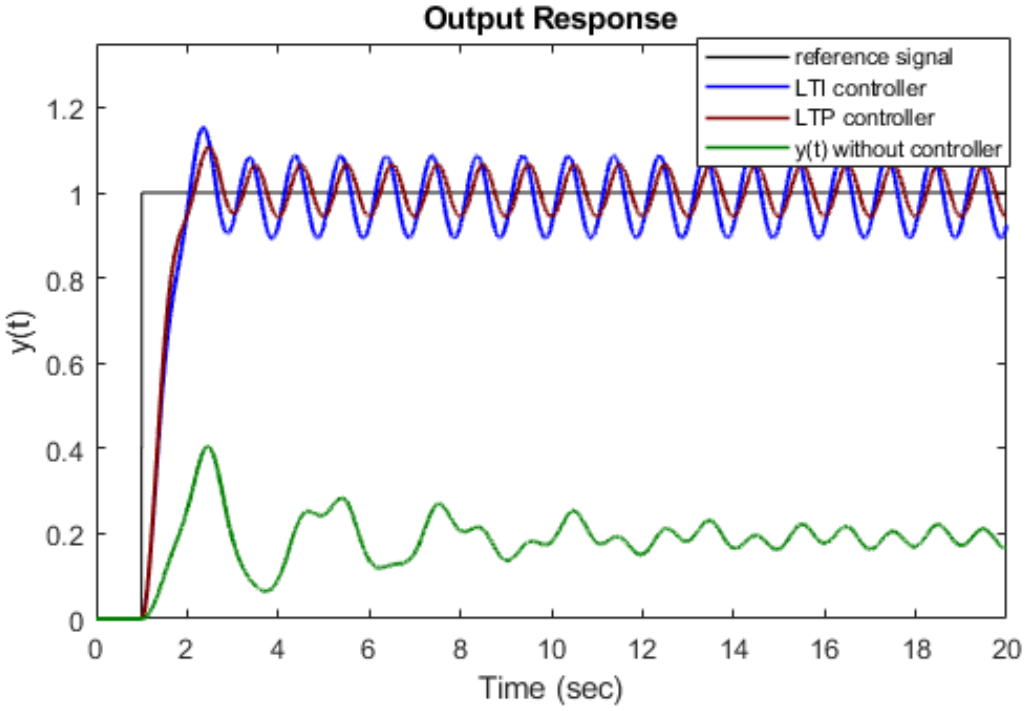

Figure 5.9 Step response of the Mathieu equation. The red signal is the step response of the precompensator LTP type LQR ($K_{p-LQR} = [6.39 + 2.9\cos(2\pi t + 0.6718), 4.3774 + 0.5086\cos(2\pi t + 1.2545)]$) and the blue signal is the step response of the precompensator-LTI type LQR ($K = [6.39, 4.3774]$) system response.

Based on the observations depicted in Fig. 5.9, it can be concluded that the LTI-LQR controller leads to larger overshoot and oscillation magnitudes in the system, while the LTP controller provides greater reduction in oscillation than the LTI controller.

Table 5.7 E_{rms} Values for LTI ($K = [6.39, 4.3774]$) and LTP type LQR controller ($K_{p-LQR} = [6.39 + 2.9\cos(2\pi t + 0.6718), 4.3774 + 0.5086\cos(2\pi t + 1.2545)]$)

	Uncontrolled	LTI Controller	LTP Controller
E_{rms}	0.8117	0.1473	0.1341

Tab. 5.7 also reports RMSE values for LTI and LTP type controllers. Note that RMSE results for the LTP type controller produce a small value compared to the LTI type controller when considering the RMSE error to the step input signal.

The application of LQR controllers, comprising LTI and LTP, has resulted in the effective stabilization and improved performance of LTP systems. Also, the time domain simulation results in Tab. 5.8 with the periodic LQR design show that the percentage overshoot decreases with a little increase in settling time.

Table 5.8 Closed loop Mathieu equation with LTP $K_{p-LQR} = [6.39 + 2.9\cos(2\pi t + 0.6718), 4.3774 + 0.5086\cos(2\pi t + 1.2545)]$) and LTI ($K = [6.39, 4.3774]$) time domain results

Controller Type	Percentage Overshoot(PO)	Settling Time (sec)
LTP	4.824	2.3
LTI	7.464	2.2

The control inputs for the velocity state, and the position state can be found in Fig .5.10. Also, in order to evaluate the ability of the system to track a sinusoidal signal, a sinusoidal input signal of the form $u_{ref(t)} = \sin(0.4t)$ was applied to the system in Fig. 5.11.

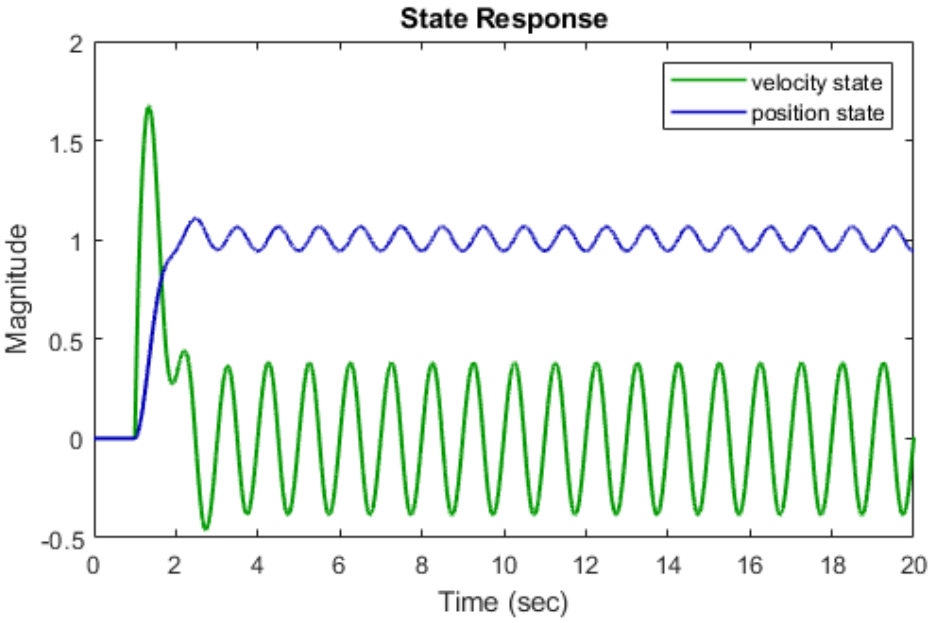

Figure 5.10 Control input signals of the closed-loop Mathieu Equation with precompensator-LQR controller. The green signal is the control input for the velocity state and the blue signal is the control input for the position state.

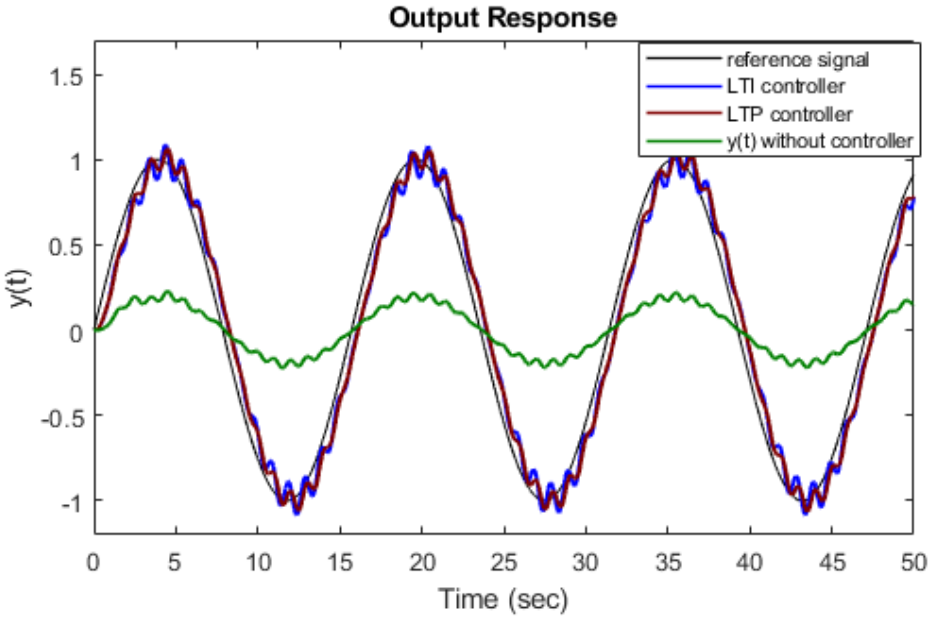

Figure 5.11 Output response of the Mathieu equation. The red signal is the response of the system with the precompensator-LTP type LQR and the blue signal is the precompensator-LTI type LQR system response and the green is the system response without any controller.

In conclusion, both classic LQR and time-varying LQR controllers are effective in stabilizing and improving the performance of linear time periodic (LTP) systems, as demonstrated by simulation results in both the time and frequency domains. The periodic LQR controller, which accounts for the periodicity of the system's behavior, provides better performance than the classic LQR controller designed for linear time-periodic (LTP) systems. This is because the time-varying LQR controller adjusts its feedback gain matrix to account for the system's periodicity, whereas the classic LQR controller uses a constant feedback gain matrix that does not consider the periodic nature of the system. These results may highlight that the periodic controllers can gain importance when more precise control strategies are necessary for the LTP systems otherwise both with the LTI or LTP type controllers the system reaches efficient time and frequency domain performances.

5.2.2. Output Response with Periodic Precompensator Gain:

The examples provided so far have involved precompensator gains that are linear time-invariant (LTI). However, in this particular case, both the precompensator gains and the LQR gains are periodic in nature. To design the precompensator gain, the weight matrices specified in Eq. (75) are utilized for analysis. The pecompensator gain $g(t)$ is calculated from the Eq. (70) and the method described in Sec. 5.1.2. The resulting precompensator gain is a periodic structure, and it is used in conjunction with the LQR gains, in Eq. (76), to achieve the desired control objectives. The calculated periodic precompensator gain in the time domain is as

$$g(t) = 11.3963 + 2.5\cos(2\pi + 2.3329)\ . \tag{78}$$

After inserting the calculated time-domain $g(t)$ matrix into the Mathieu equation in MATLAB/Simulink environment the step response of the system can be found in Fig. 5.12. A reference step input was applied to the system at $t = 1$ second, and the input was sustained for a duration of 10 seconds.

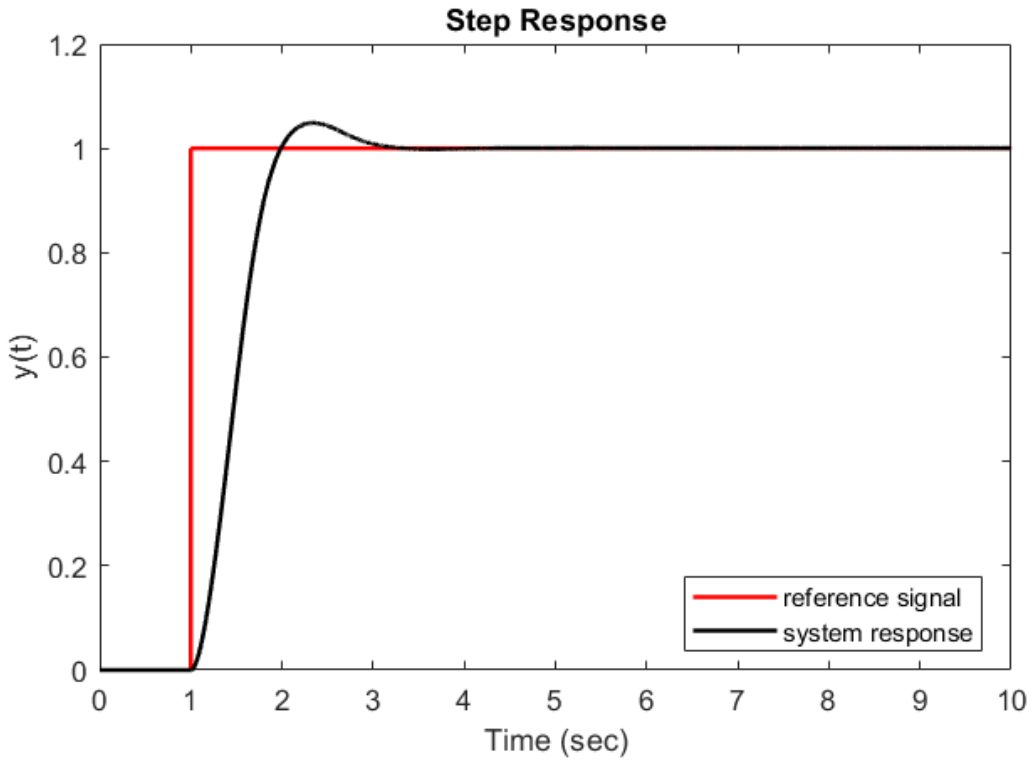

Figure 5.12 Step response of the closed loop Mathieu equation with periodic precompensator ($g(t) = 11.3963 + 2.5\cos(2\pi + 2.3329)$) gain and LTP-LQR controller. The black signal is the reference step input signal that was applied to the system at $t = 1$ second, and the blue signal is the step response of the closed loop Mathieu equation.

The system's performance improvements were verified through time-domain simulations, and the RMSE value between the reference step signal and the system output was found to be 0.1346. As seen in Fig. 5.13 the periodic precompensator gain and LTP-LQR controller successfully compensate the periodic effect by modifying the input signal with the periodic frequency.

The control inputs for the velocity state, and the position state can be found in Fig .5.18. Also, in order to evaluate the ability of the system to track a sinusoidal signal, a sinusoidal input signal of the form $u_{ref}(t) = \sin(0.5t)$ was applied to the system, and the related output response graph is presented in Fig. 5.14.

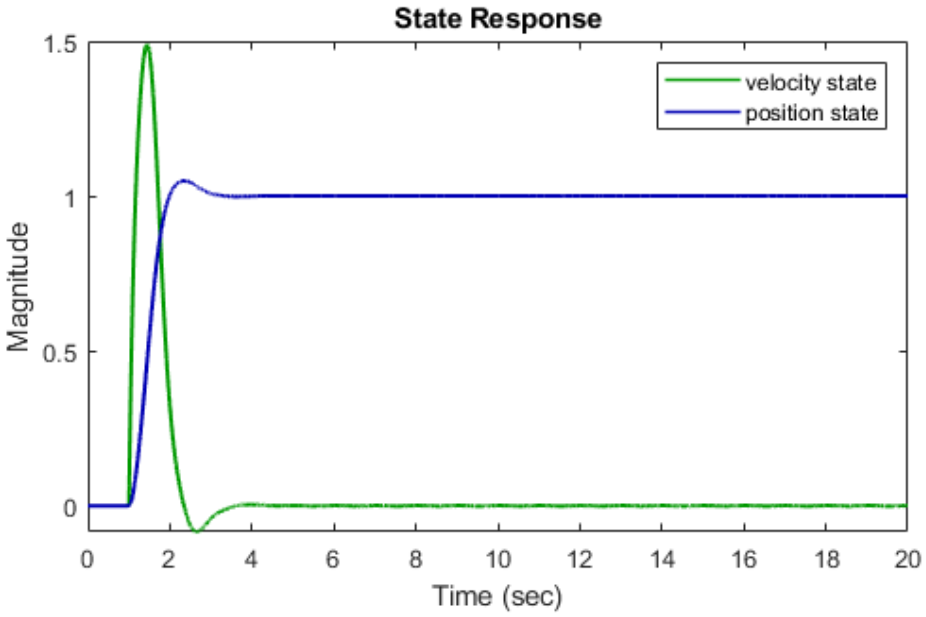

Figure 5.13 Control input signals of the closed-loop Mathieu equation with periodic-precompensator LQR controller. The green signal is the control input for the velocity state and the blue signal is the control input for the position state.

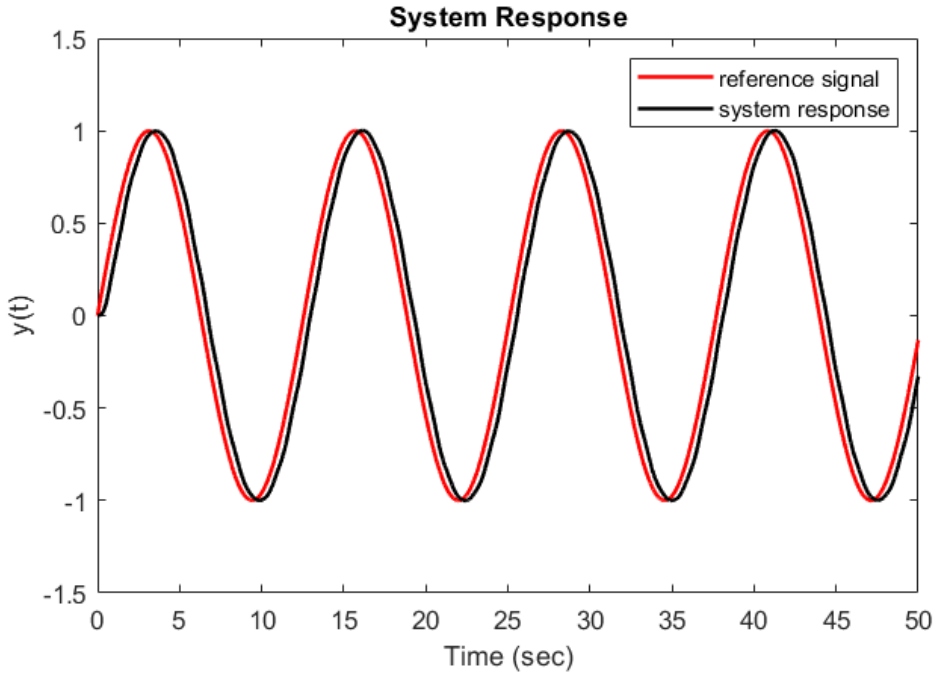

Figure 5.14 Output response of the closed loop Mathieu equation with periodic pre-compensator periodic-LQR controller $(g(t) = 11.3963 + 2.5\cos(2\pi + 2.3329))$.

The related time domain performance results in terms of percentage overshoot and settling time are represented in Tab. 5.9.

Table 5.9 Closed loop Mathieu equation with $(g(t) = 11.3963 + 2.5\cos(2\pi + 2.3329))$ time domain results

Controller Type	Percentage Overshoot(PO)	Settling Time (sec)
LTP	4.9	3.7

In the given closed-loop system, the periodic precompensator gains are found to be effective in improving the system's performance. By utilizing these gains, the system's phase margin increases to the value of $154\ degree$, Bandwidth to the value of $2.53\ rad/sec$, and delay margin to the value of $10.3\ sec$, the calculations based on the fundamental harmonic H_0. This controller structure with periodic precompensator gain results in a reduction of overshoot to the 4.9% and an increase in the settling time to the value of $3.7\ sec$. Also most important property, we can handle the harmonics of the system so the system stopped oscillation, and we observed nearly zero steady-state error.

The process of designing a Linear Quadratic Regulator (LQR) poses a significant challenge in selecting appropriate weight matrices, which play a crucial role in the overall performance of the control system. To come up with a general understanding of the variation of weight matrices, we performed different examples and related results are presented in Fig .5.15 and Fig .5.16.

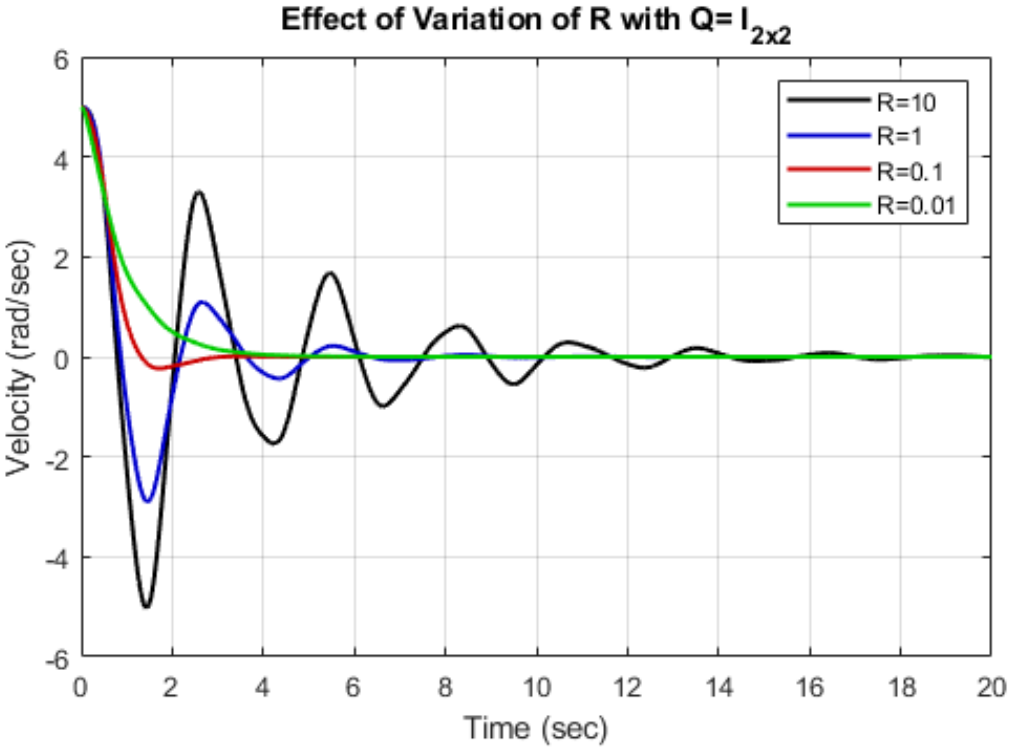

Figure 5.15 Zero input response of the closed loop Mathieu equation with precompensator LTP-LQR controller. Effects of variation R was given with a constant $Q = I_{2X2}$ matrix

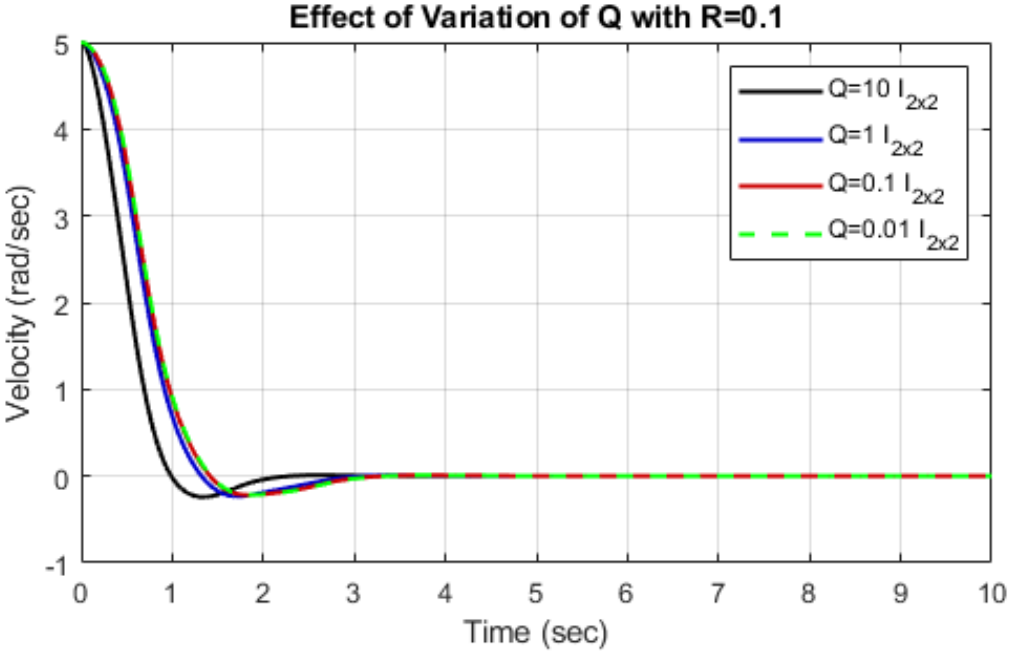

Figure 5.16 Zero input response of the closed loop Mathieu equation with precompensator LTP-LQR controller. Effects of variation Q was given with a constant $R = 0.1$

To investigate the effects of variation of R, we keep Q as the identity matrix and only alter R. When the R matrix is increased, the control system will place more emphasis on minimizing the control effort. This can result in smoother control actions and less energy consumption, but it may also cause the system to take longer to reach the desired state or not achieve the desired performance. As seen from Fig. 5.15 larger value for R causes oscillation, bigger overshoot, higher settling time, and rise time. Similarly, selecting a higher value for Q indicates that, the control system will place more emphasis on minimizing the error in the state variables. This can result in more aggressive control actions and faster convergence to the desired state, but it may also cause the system to become less stable or more sensitive to disturbances. When both matrices are increased, the effects will be a trade-off between them. The system will tend to be more aggressive, less smooth, and will consume more energy.

It's important to note that the optimal values for the weight matrices depend on the specific requirements and constraints of the controlled system and are typically determined through trial and error calculations.

5.2.3. LQI Controller Validation on Mathieu Equation

In this section, we used the Linear Quadratic Integrator (LQI) method described in Fig .5.2 structure to investigate the effects of the periodic LQI controller on a simulation environment and mentioned the regulation (stabilization) and reference tracking performances of the closed loop system. As explained in the previous chapter, we can achieve better dynamics, stability, and performance results by using precompensator structure so the LQI structure can be thought of as an alternative method.

Periodic LQI controller was designed with the same weight matrices in Eq .(75) and after the manual tuning for the integrator gain on the simulation platform, we chose to use the integral gain as $K_i = 12.35$.

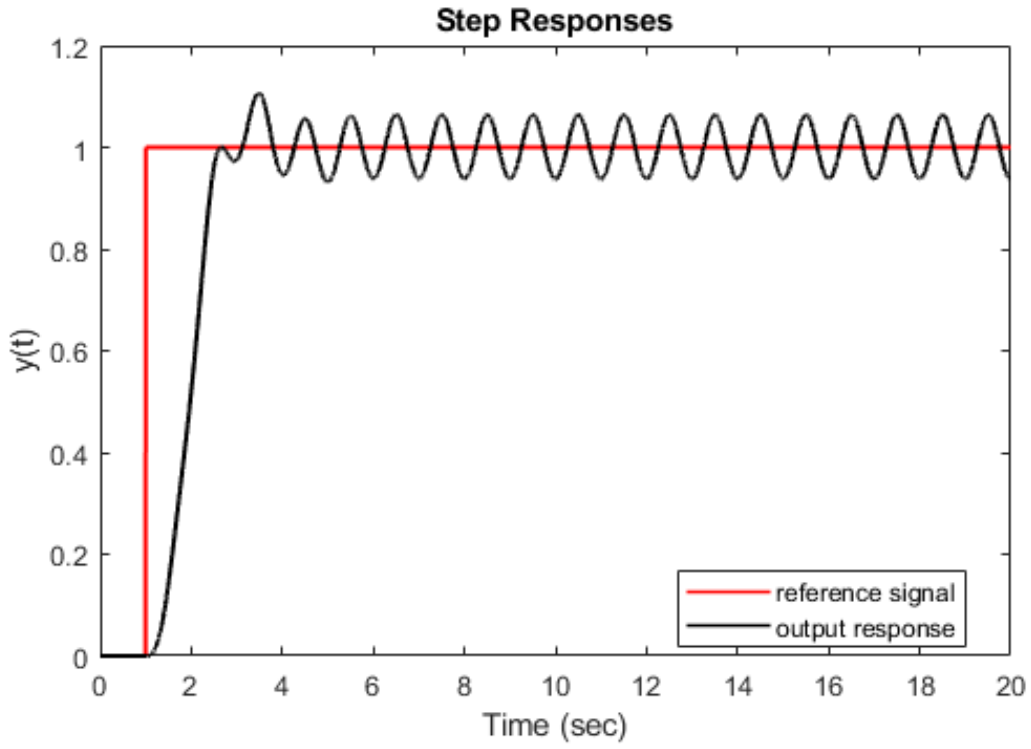

Figure 5.17 Step response of the closed loop Mathieu equation with periodic-LQI controller.

Table 5.10 Frequency domain of the closed loop Mathieu equation with periodic-LQI controller.

Phase Margin (degree)	Delay Margin (sec)	Bandwidth (rad/sec)
69.2	0.657	2.3

The control inputs for the velocity state, and position state can be found in Fig .5.18.

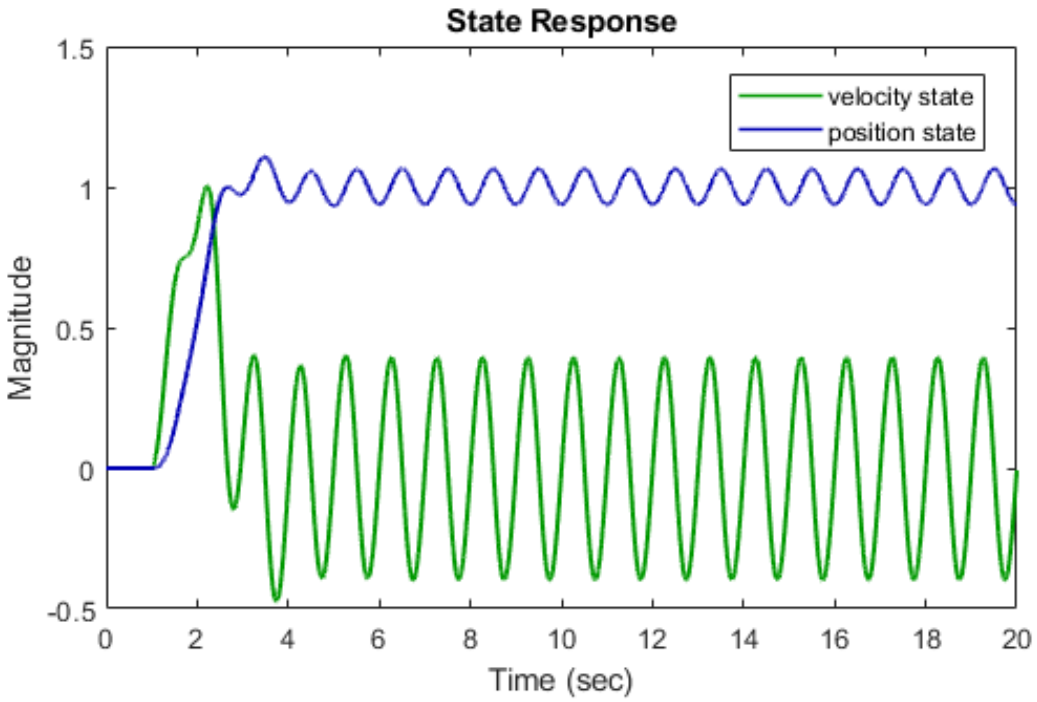

Figure 5.18 Control input signals of the closed-loop Mathieu equation with periodic-LQI controller. The green signal is the control input for the velocity state and the blue signal is the control input for the position state.

After the LQI controller is deployed to the system, the phase margin increases to the value of $69.2degree$, delay margin $0.657sec$, and Bandwidth $2.3rad/sec$, in detailed can be seen in Tab. 5.10. The related bandwidth, delay margin, and phase margin values are calculated from the fundamental harmonic (H_0). The step signal was applied to the system for reference tracking analysis the resulting output response of the system is in Fig. 5.17. The percentage overshoot is about 50 and the settling time is $4.558sec$. Also, the resulting RMSE value for the reference step input and the closed loop system response is equal to 0.2013 which is greater than the results with precompensator gain. Both results in the time-domain and frequency-domain are worst than precompensator LQR configurations.

By comparing the closed-loop simulation results of the Mathieu equation, we executed different LQR controller structures and LQI examples with both time-invariant and time-periodic designs. It can be concluded that the use of the LQR controllers significantly

improves the stability, robustness, time, and frequency domain performance of the LTP system.

5.3. Controller Design and Validation: LTP Test Platform

It is necessary to check the controllability and observability of the system model before the controller implementation process. The ability to control the state to reach a desired final value from an initial state through the application of an acceptable control effort is known as controllability. The controllability of the system can be determined by examining the rank of the controllability matrix C. If the rank of C is full, then the system is considered controllable, meaning that for any initial state, the system can be steered to any desired final state within a finite time period. In the present case, as the system has two states based on the results of the parametric identification, the controllability matrix C can be determined as,

$$C = [B|AB] \tag{79}$$

Since the system matrices are in the Teoplitz form of system matrices A, B, C and D the controllability matrix has the dimension of 6×6 and it is expressed as:

$$C = \begin{bmatrix} 0 & 0 & 28142 & 0 & 0 & 0 \\ 28142 & 0 & 0 & -3.1\ 10^6 + 3.5\ 10^5 i & 0 & 0 \\ 0 & 0 & 0 & 0 & 28142 & 0 \\ 0 & 28142 & 0 & 0 & -3.1\ 10^6 & 0 \\ 0 & 0 & 0 & 0 & 0 & 28142 \\ 0 & 0 & 281420 & 0 & 0 & -3.1\ 10^6 + 3.5\ 10^5 i \end{bmatrix}. \tag{80}$$

Since the controllability matrice C has full rank and the system is controllable.

The concept of observability refers to the system's capability of determining its internal states by monitoring the output over a finite period of time. The system is considered observable if and only if the observability matrix has full rank.

The observability matrix is defined as

$$O = \begin{bmatrix} C \\ CA \end{bmatrix} \tag{81}$$

So the observability matrix is calculated as

$$O = \begin{bmatrix} 1 & 0 & 0 & 0 & 0 & 0 \\ 0 & 0 & 1 & 0 & 0 & 0 \\ 0 & 0 & 0 & 0 & 1 & 0 \\ 0 & 1 & 0 & 0 & 0 & 0 \\ 0 & 0 & 0 & 1 & 0 & 0 \\ 0 & 0 & 0 & 0 & 0 & 1 \end{bmatrix} \tag{82}$$

Since the rank of the observability matrix is 6 and it has full rank so the system is observable.

5.3.1. Experimental Validation of Controllers on the Physical Test Platform

The validation task of an LQR controller on an LTP test platform involves evaluating the performance of the controller under different operating conditions and comparing it with the desired performance metrics. This involves evaluating the system's response to disturbances, changes in operating conditions, and other factors that may affect the system's performance.

In this section, we present the performance results of controllers on the physical test platform of the LTP system. This allows for a more accurate evaluation of the controller's performance in a real-world environment. During experiments, it is important to use appropriate performance metrics to quantify the controller's performance. These metrics may include the settling time, the steady-state error, the overshoot, the control efforts, etc. It's worth noting that the validation process is an iterative process, and manual adjustments to the controllers may be needed to achieve the desired performance.

a. Case Study #1,

A periodic LQI controller was designed based on the below conditions. For the first experiment, the weight matrices are chosen as

$$\begin{aligned} R &= 0.01 \\ Q &= \begin{bmatrix} 0.1 & 0 \\ 0 & 0.0001 \end{bmatrix} \end{aligned} \tag{83}$$

After manual tuning on the test platform, the Integrator Gain was chosen as 23, and the resulting LQI gain matrix was calculated as in Eq. 84, which is computed by solving the ARE equation. The obtained matrix has the Toeplitz form so by taking the middle column of the K_{LQR} matrix as in Fig. 4.1 the following matrix can be obtained:

$$K_{p-LQR} = \begin{bmatrix} -0.0204 + 0.0001i & -0.0000 + 0.0000i \\ 0.9114 + 0.0000i & 0.0289 + 0.0000i \\ -0.0204 - 0.0001i & -0.0000 - 0.0000i \end{bmatrix} \tag{84}$$

By using the rule in Sec. 5.1.2. the periodic K_{p-LQR} gain matrix is found as

$$K_{p-LQR} = [0.9114 - 0.0408\cos(4\pi t), 0.0289] \tag{85}$$

Also, the LTI controller is as

$$K_{LQR} = [0.9114, 0.0289] \tag{86}$$

The closed loop output response with the periodic K_{p-LQR} gains to a sine input signal is given in Fig. 5.19.

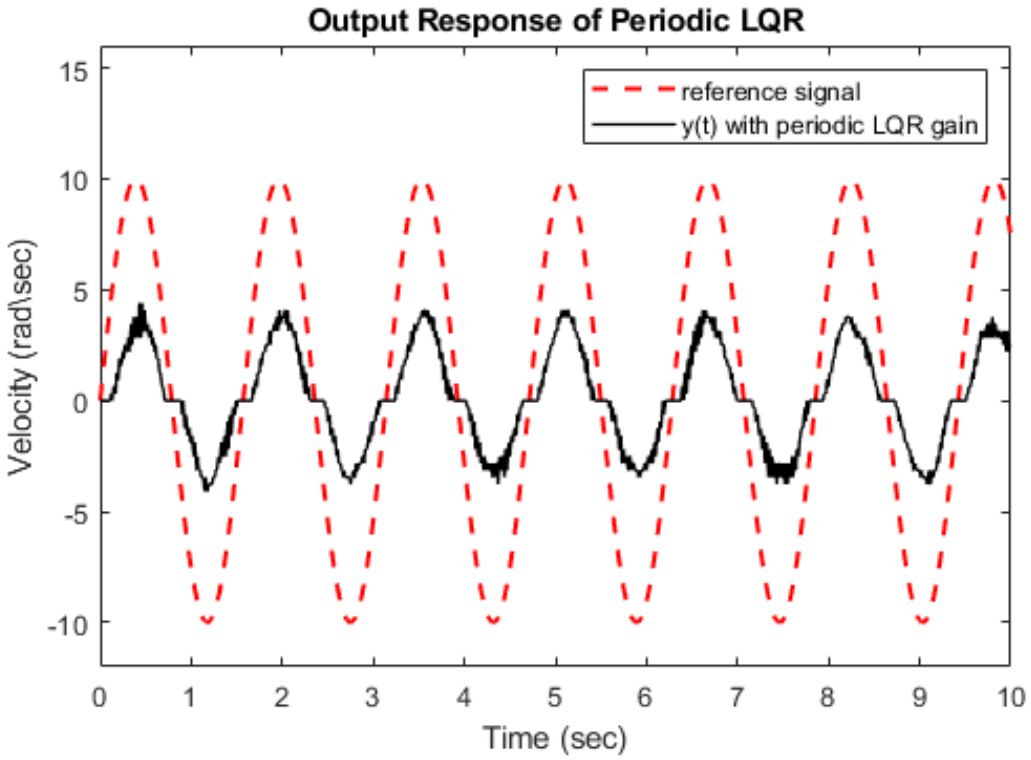

Figure 5.19 Closed loop system with periodic-LQR with input 4 rad/sec sine input signal.

To analyze the ability of the controller to track the reference signal is tested by providing a sinusoidal signal with different magnitudes and frequencies. Fig. 5.20 and Fig. 5.21 show the tracking performance of the control scheme for $u_{ref}(t) = 10\sin(4t)$ and $u_{ref}(t) = 20\sin(6t)$ reference signals, respectively.

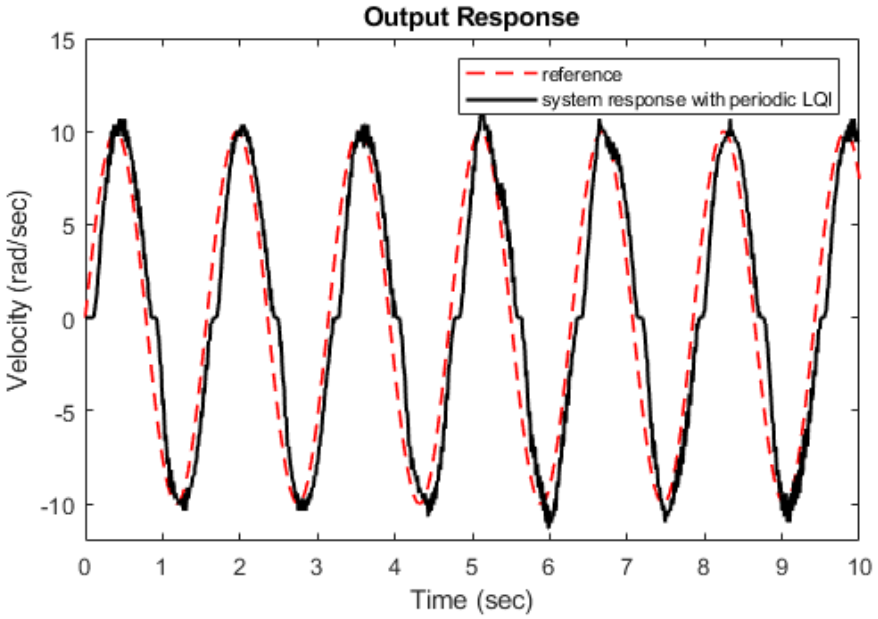

Figure 5.20 Closed loop system response with periodic LQI gain $K_{p-LQR} = [0.9114 - 0.0408\cos(4\pi t), 0.0289]$ and 23 integrator gain in the time domain to an input signal $u_{ref}(t) = 10\sin(4t)$.

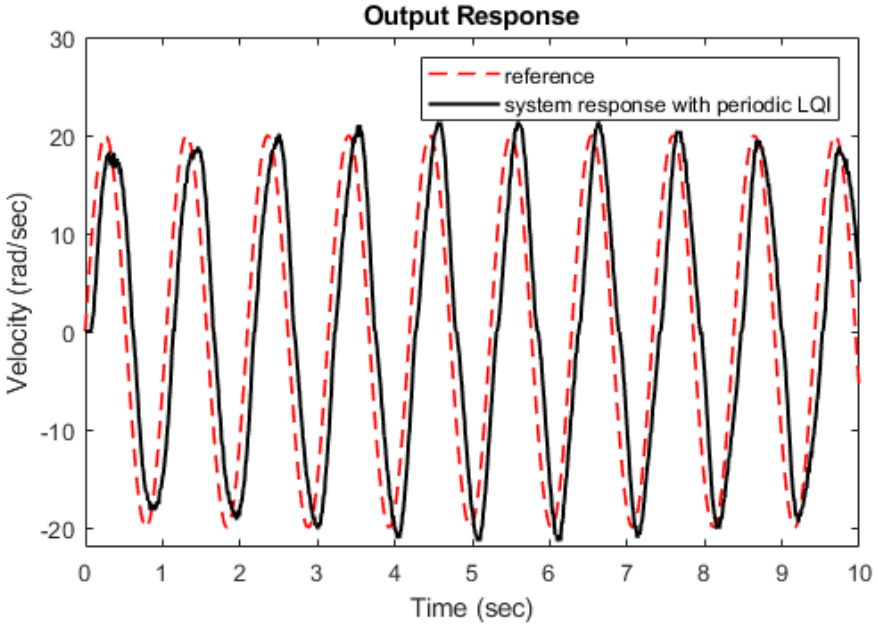

Figure 5.21 Closed loop system response with periodic LQI gain $K_{p-LQR} = [0.9114 - 0.0408\cos(4\pi t), 0.0289]$ and 23 integrator gain in the time domain to an input signal $u_{ref}(t) = 20\sin(6t)$.

From the tracking performance results in Fig. 5.20 and Fig. 5.21, it is observed that the closed loop system is robust to the reference signal changes in both magnitude and phase.

After inserting the calculated time-domain K_{p-LQR} matrix and integrator gain K_i into the test platform equation in MATLAB/Simulink environment the step response of the system can be obtained as in Fig. 5.22. A reference step input was applied to the system at $t = 0.3\ sec$, and the input was sustained for a duration of $10\ sec$.

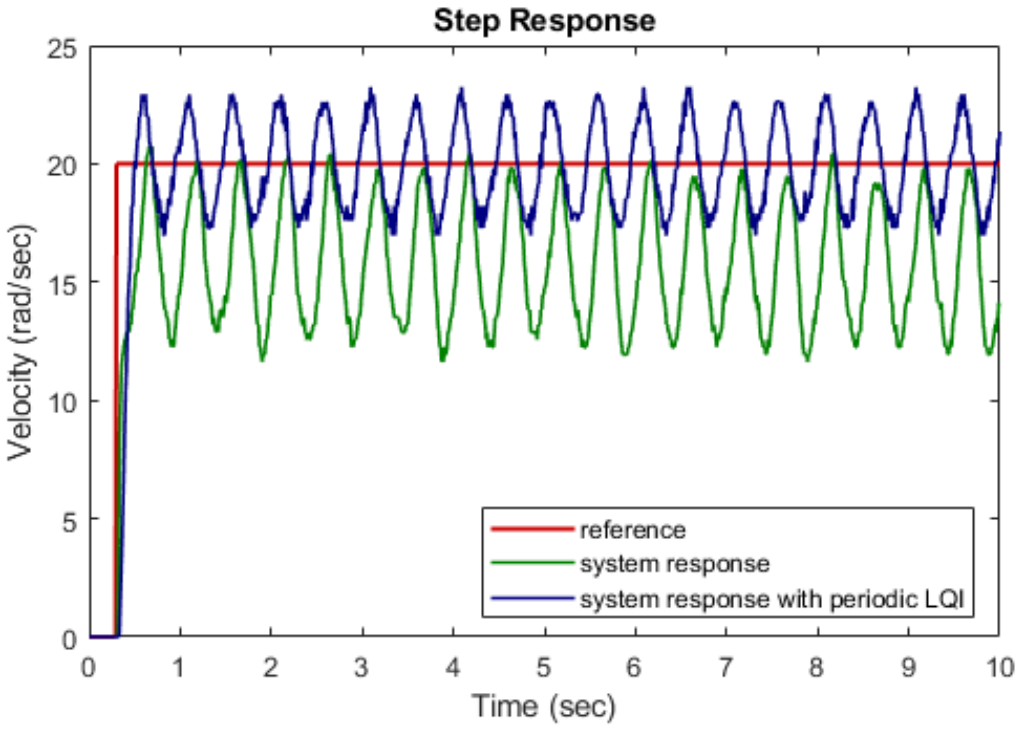

Figure 5.22 Step response of the LTP test platform. The blue signal is the step response of the system with periodic (LQI) gain $K_{p-LQR} = [0.9114 - 0.0408\cos(4\pi t), 0.0289]$ and 23 integrator gain. The green signal is the step response of the LTP test platform without any controller.

The blue response is the response of the LTP test system with the LQI controller and the green is the open loop response of the test platform without any controller. All the response data were collected from the physical test system so there are some noise and some delays in the results. As can be seen from the graph in Fig. 5.22, the LQI controller will adjust the system's inputs in real-time in order to minimize the error between the desired output and

the actual output of the system. This can improve the overall stability and performance of the system.

Table 5.11 E_{rms} values for LTI ($K_{LQR} = [0.9114, 0.0289]$) and LTP-LQI $K_{p-LQR} = [0.9114 - 0.0408\cos(4\pi t), 0.0289]$ controller

	Uncontrolled	LTP Controller	LTI Controller
E_{rms}	0.2546	0.1174	0.1157

The table provided in Tab. 5.11 displays the RMSE values for both LTI and LTP systems with controllers, as well as a reference signal. From the results, it is clear that the use of LQR controllers leads to improvements in the performance of the system. Nonetheless, due to the presence of physical system disturbances (such as noise, friction, etc.), it is challenging to distinguish substantial differences between LTI and LTP-type LQI controllers. The RMSE values show only a minor variance between the two types of controllers.

b. Case Study #2

For a second case study, the weight matrices R and Q chosen for the LQI design are

$$\begin{aligned} R &= 0.1 \\ Q &= \begin{bmatrix} 0.5 & 0 \\ 0 & 0.0001 \end{bmatrix} \end{aligned} \tag{87}$$

After the necessary mathematical calculations that are explained in Sec. 5.1.2. the LTP-LQR gain is calculated as

$$K_{p-LQR} = [2.1448 + 0.0432\cos(4\pi t - 3.1277), 0.0302] \tag{88}$$

Also, the calculated LTI-LQR gain is as

$$K_{LQR} = [2.1448, 0.0302] \tag{89}$$

After manual tuning on the physical test platform, the Integrator Gain was chosen as 30.

In order to investigate the response of the system to different frequency signals, two types of signals were utilized for a duration of 10 seconds. Initially, a sinusoidal signal in the form of $u_{ref}(t) = 10\sin(4\pi t)$ was applied to the system, followed by a square wave with $u_{ref}(t) = 10square(3\pi t)$.

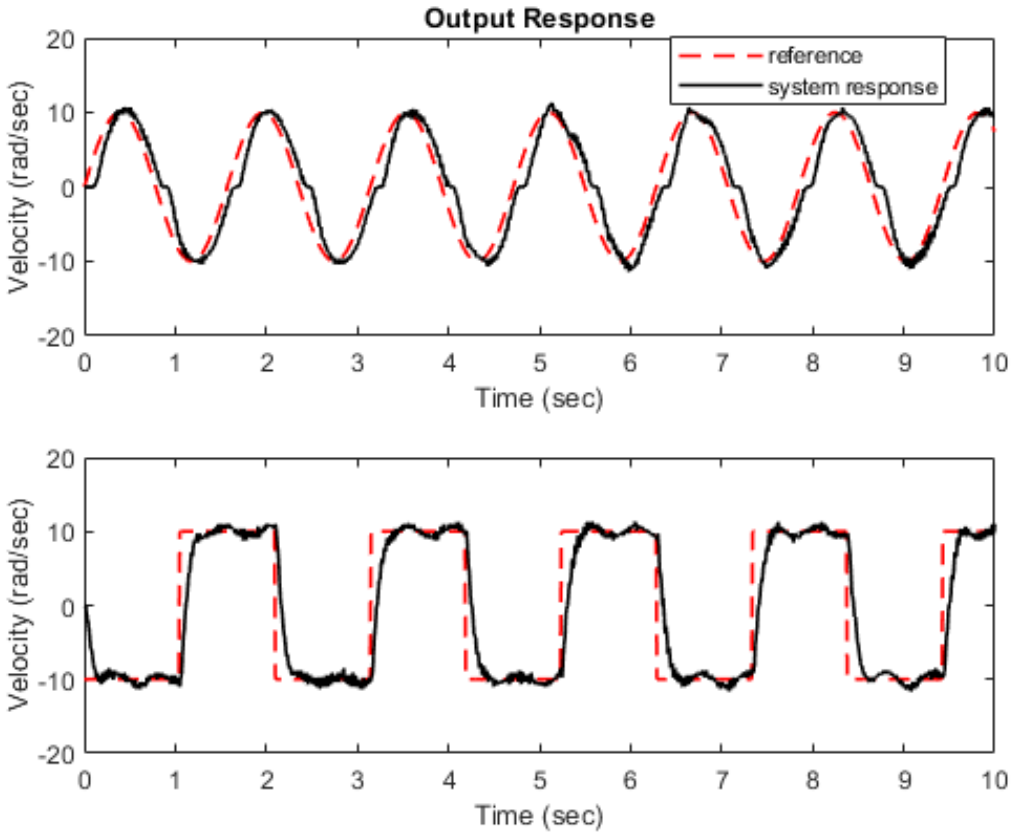

Figure 5.23 Closed loop system response with periodic (LQI) and a 30 integrator gain in the time domain simulations. The first graph is the output response of the closed loop system with $u_{ref}(t) = 10\sin(4t)$, and the second graph is the closed loop output response of $u_{ref}(t) = 10square(3t)$input signal.

The performance of an LQI controller can be assessed by evaluating its reference tracking capability using both square and sine wave input signals, as depicted in Fig. 5.23. The results showed that the LQI structure can achieve good tracking performance for different input signals in a physical environment. However, the saturation non-linearity of the system may

cause dead-zone areas to appear at specific points. Nevertheless, the results demonstrate that the LQI controller is effective in tracking reference signals despite the presence of nonlinearities.

For analyzing the step response of the closed loop system, the reference step input was applied to the system at $t = 0.3$ second, and the input was sustained for a duration of 10 seconds. The related step response of the system is given in Fig. 5.24.

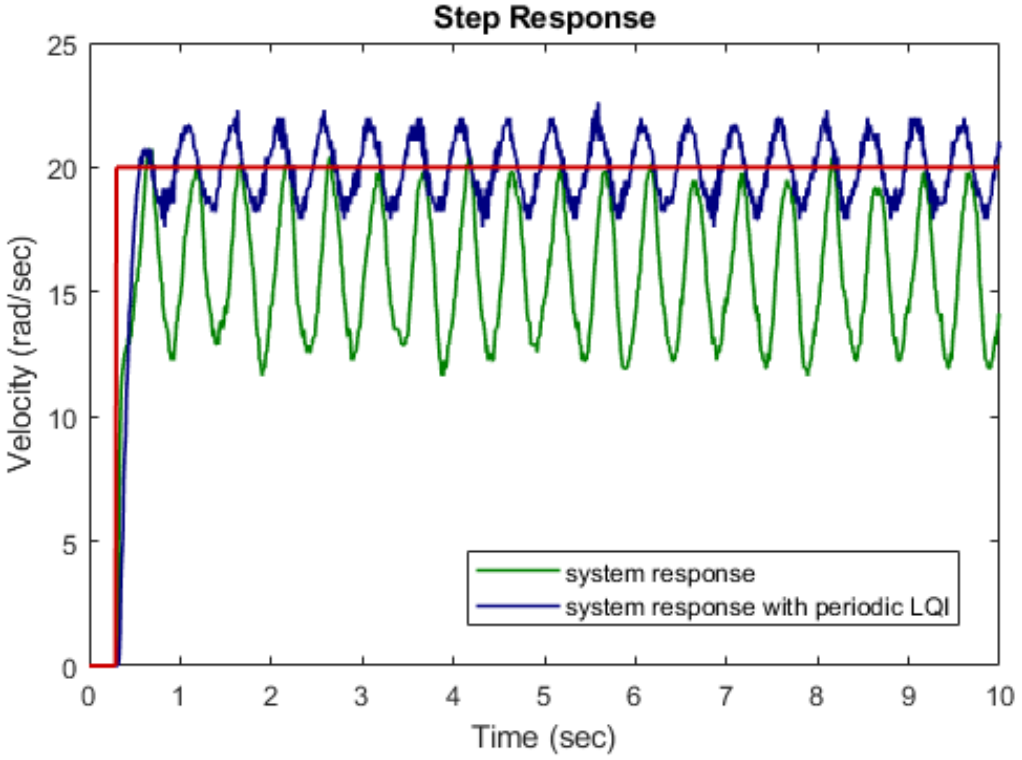

Figure 5.24 Step response of the LTP test platform. The blue signal is the step response of the system with periodic (LQI) gain $K_{p-LQR} = [2.1448 + 0.0432\cos(4\pi t - 3.1277), 0.0302]$ and 30 integrator gain. The green signal is the step response of the LTP test platform without any controller.

Table 5.12 RMSE values for LTI ($K_{LQR} = [2.1448, 0.0302]$) and LTP type LQR ($K_{p-LQR} = [2.1448 + 0.0432\cos(4\pi t - 3.1277), 0.0302]$) controller

	Uncontrolled	LTI Controller	LTP Controller
E_{rms}	0.2546	0.1110	0.1098

Tab. 5.12 compares the RMSE values for both LTI and LTP systems with controllers, along with a reference step signal. The results indicate that the use of LQR controllers has a positive impact on the system's performance the same as in other experiments. Also, the E_{rms} values demonstrate that there is only a slight difference between the two types of controllers.

5.3.2. Output Response with Precompensator Gain

In this section, the LQR and precompensator gain matrices were computed using the weight matrices presented in Eq.(83) and the formula described in Eq. (70). The corresponding LQR gain matrix is the same as the one shown in Eq.(84). Since the calculated periodic gains of the precompensator are minimal and have no significant impact on the output response, all the precompensator gains were designed and tested in LTI form. After obtaining the precompensator g, we fine-tuned it manually to achieve better tracking performance.

The calculated precompensator gain is equal to 2.2.

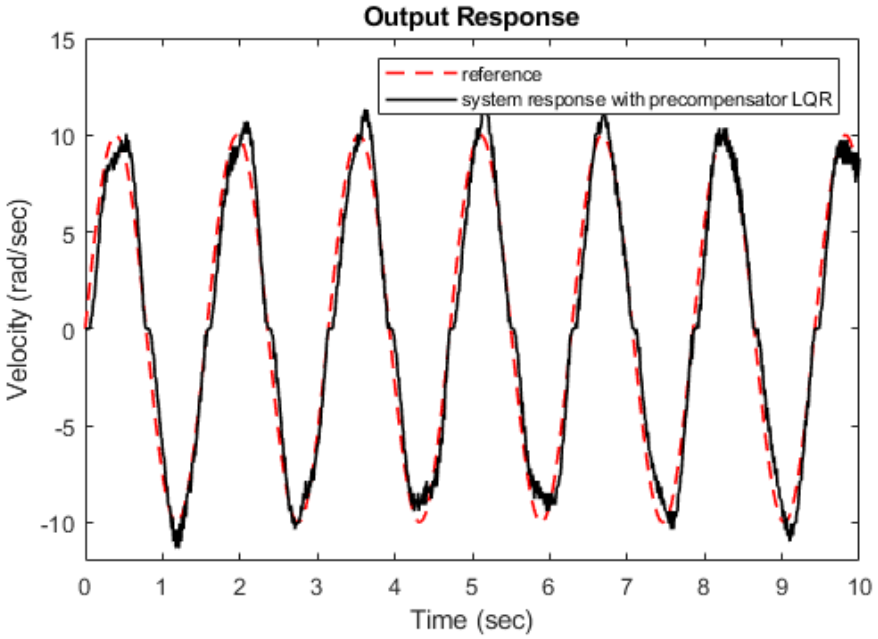

Figure 5.25 Closed loop system response with 2.2 pre-compensator periodic (LQR) gain configuration $K = [0.9114 - 0.0408\cos(4\pi t), 0.0289]$ in the time domain to an input signal $u_{ref}(t) = 10\sin(4t)$.

The system successfully tracks the reference input signal as can be seen in the output graph in Fig. 5.25. Different from Mathieu equation examples, we did not observe the periodic precompensator gain results because of the physical limitations of the test platform. But with the LTI form precompensator gains we observe good reference tracking performance.

6. CONCLUSIONS AND FUTURE WORK

Linear time-periodic (LTP) systems are commonly found in various critical systems, including wind turbines, walking/running robotics, helicopter rotors, power networks, and nonlinear systems when linearized around periodic orbits. Despite being extensively studied in the literature, there are limited techniques for identifying LTP systems from input/output data. Analytical solutions for LTP systems can be complex and challenging, making experimental methods an appealing alternative. In this thesis, two different Linear Time Periodic (LTP) systems were utilized to validate the identification and control design methods.

In the first part of this thesis, the periodic Mathieu equation was utilized as a simulation case study, and its state-space representation was implemented in a MATLAB/Simulink environment. The system was stimulated with constant-frequency cosine signals, and the resulting output data was analyzed to conduct data-driven identification methods. Harmonic Transfer Functions (HTFs) were estimated from the data, and their prediction performance was compared to that of theoretically calculated HTFs. Furthermore, the accuracy of the estimation method was evaluated by comparing the output estimation results from the estimated HTFs to those obtained from the theoretical methods.

In the second part of this thesis, we developed a test bench for system identification and control for linear time-periodic (LTP) systems. We used a coupled DC motor system to imitate a periodic load, which admits an LTP state-space realization. We used Matlab/Simulink hardware support libraries to allow the programming of the test bench in Matlab/Simulink environment with a low-cost solution. We used constant-frequency sinusoids to estimate the harmonic transfer functions (HTFs) of the experimental system. We also perform parametric system identification techniques in order to analyze the system in the simulation environment. Using the reference parametric state-space model, we utilized gray-box system identification to estimate the unknown parameters of the test platform by using optimization functions.

Finally, we focused on periodic controller design for LTP systems. In this regard, LQR controllers were chosen as they are widely used in LTP systems. Initially, the controller designs were validated using the Mathieu equation. We introduced a method for obtaining periodic controllers from the classical methods of the solution of ARE equations. We also performed our analysis with different periodic LQR controller structures to enhance our systems. The first configuration is the LQR design with precompensator gain. The precompensator gains were also tested both in LTI and LTP structures. We discussed the time-invariant and time-periodic controllers in terms of system metrics in frequency and time domain analysis. After that, we performed the same control strategies on the physical LTP test platform. Since we have the system parameters, that we have already derived in parametric identification methods, we designed periodic LQR controllers with different structures, precompensator LQR and LQI. We validated all controller structures on the LTP test platform. We gave the performance metrics for LTI and LTP type controllers with the physical LTP test platform. We observe different behaviors for different control structures and compared them with different metrics such as RMSE calculations between the reference signal and the system output, overshoot results or settling time values, etc. In our case studies, we can not exactly say that we have to use periodic controllers for LTP systems. Because, both LTI-LQR and time-varying LQR controllers are both effective in stabilizing and improving the performance of linear time periodic (LTP) systems, as demonstrated by simulation results in both the time and frequency domains. But these results may highlight that the periodic controllers can gain importance when more precise control strategies are necessary for the LTP systems otherwise both with the LTI or LTP type controllers the system reaches efficient time and frequency domain performances. Also from our case studies on the Mathieu equation, we can say that the periodic precompensator controller works better than the other configurations for Mathieu system analysis. Unfortunately, we were unable to examine all possible configurations on the physical LTP platform due to system limitations, including saturation and dead zones, etc. in the motor system.

As a future work, the study and periodic control of various physical systems, such as legged robots, missile control systems, or biological rhythmic locomotor systems, can be done using

the data-driven system identification or parametric identification approaches given in this thesis. The controller design methods explained in this thesis will also open the door for the periodic control of LTP systems. There are recent subspace-based state-space identification techniques for LTP systems [19]. Using these techniques for the system identification part in the future may eliminate the need for a gray-box model of the system for parametric system identification.

REFERENCES

[1] Miklós Farkas. *Periodic motions*, volume 104. Springer Science & Business Media, **2013**.

[2] Henrik Sandberg, Erik Mollerstedt, and Bo Bernhardsson. Frequency-domain analysis of linear time-periodic systems. *IEEE Transactions on Automatic Control*, 50(12):1971–1983, **2005**.

[3] Matthew S Allen, Michael W Sracic, Shashank Chauhan, and Morten Hartvig Hansen. Output-only modal analysis of linear time-periodic systems with application to wind turbine simulation data. *Mechanical Systems and Signal Processing*, 25(4):1174–1191, **2011**.

[4] D. L. Sheu. Wind energy conversion. volume vii. effects of tower motion on the dynamic response of windmill rotor. doi:10.2172/5546242.

[5] Erik Mollerstedt and Bo Bernhardsson. A harmonic transfer function model for a diode converter train. In *Power Engineering Society Winter Meeting, 2000. IEEE*, volume 2, pages 957–962. IEEE, **2000**.

[6] Möllerstedt, Erik. *Dynamic Analysis of Harmonics in Electrical Systems*. Ph.D. thesis, Lund University, **2000**.

[7] Rafael Z. Scapini, Lucas Vizzotto Bellinaso, and Leandro Michels. Stability analysis of ac–dc full-bridge converters with reduced dc-link capacitance. *IEEE Transactions on Power Electronics*, 33:899–908, **2018**.

[8] Sunghwan Hwang. *Frequency Domain System Identification of Helicopter Rotor Dynamics Incorporating Models With Time Periodic Coefficients*. Ph.D. thesis, Graduate School of the University of Maryland at College Park, **1997**.

[9] P. Friedmann, C. E. Hammond, and Tze-Hsin Woo. Efficient numerical treatment of periodic systems with application to stability problems. *International Journal*

for Numerical Methods in Engineering, 11(7):1117–1136, **1977**. doi:https://doi.org/10.1002/nme.1620110708.

[10] John Dugundji and John H. Wendell. Some analysis methods for rotating systems with periodic coefficients. *AIAA Journal*, 21(6):890–897, **1983**. doi:10.2514/3.8167.

[11] Afreen Siddiqi. *Identification of the harmonic transfer functions of a helicopter rotor*. Master's thesis, Massachusetts Institute of Technology, **2001**.

[12] Bernhard P Lampe and Efim N Rosenwasser. Standardizability of linear periodic sampled-data systems. *IFAC-PapersOnLine*, 49(14):166–171, **2016**.

[13] Ismail Uyanik. *Identification of legged locomotion via model-based and data-driven approaches*. Ph.D. thesis, Bilkent University, **2017**.

[14] JA Richards. The mathieu equation. In *Analysis of Periodically Time-Varying Systems*, pages 93–107. Springer, **1983**.

[15] Gaston Floquet. Sur les équations différentielles linéaires à coefficients périodiques. In *Annales scientifiques de l'École normale supérieure*, volume 12, pages 47–88. **1883**.

[16] Norman M Wereley. *Analysis and control of linear periodically time varying systems*. Ph.D. thesis, Massachusetts Institute of Technology, **1990**.

[17] Ismail Uyanik, Mustafa M Ankarali, Noah J Cowan, Uluc Saranli, and Omer Morgul. Identification of a vertical hopping robot model via harmonic transfer functions. *Transactions of the Institute of Measurement and Control*, 38(5):501–511, **2016**.

[18] Elvan Kuzucu Hidir, Ismail Uyanik, and Omer Morgul. Harmonic transfer functions based controllers for linear time-periodic systems. *Transactions of the Institute of Measurement and Control*, 41(8):2171–2184, **2019**.

[19] Ismail Uyanik, Uluc Saranli, Mustafa Mert Ankarali, Noah J Cowan, and Omer Morgul. Frequency-domain subspace identification of linear time-periodic (ltp) systems. *IEEE Transactions on Automatic Control*, 64(6):2529–2536, **2018**.

[20] Laurent Mevel, Ivan Gueguen, and Dmitri Tcherniak. Lptv subspace analysis of wind turbines data. In *EWSHM-7th European Workshop on Structural Health Monitoring*. **2014**.

[21] K. Liu. Identification of linear time-varying systems. *Journal of Sound and Vibration*, 206(4):487–505, **1997**. ISSN 0022-460X. doi:https://doi.org/10.1006/jsvi.1997.1105.

[22] Jocelyn Sabatier, Alain Oustaloup, Aitor Garcia Iturricha, and François Levron. Crone control of continuous linear time periodic systems: Application to a testing bench. *ISA transactions*, 42(3):421–436, **2003**.

[23] MV Bartuccelli, G Gentile, and KV Georgiou. On the dynamics of a vertically driven damped planar pendulum. *Proceedings of the Royal Society of London. Series A: Mathematical, Physical and Engineering Sciences*, 457(2016):3007–3022, **2001**.

[24] İsmail Uyanık and Bahadir Catalbas. A low-cost feedback control systems laboratory setup via arduino-simulink interface. *Computer Applications in Engineering Education*, 26, **2018**. doi:10.1002/cae.21917.

[25] Elvan Kuzucu Hıdır. *Identification, stability analysis and control of linear time periodic systems via harmonic transfer functions*. Master's thesis, Bilkent University, **2017**.

[26] F. Demet Ulker. *A New Framework For Helicopter Vibration Suppression; Time-Periodic System Identification and Controller Design*. Ph.D. thesis, Carleton University, **2011**.

[27] Carlos A. Malpica. *Contributions to the dynamics of helicopters with active rotor controls*. Ph.D. thesis, University of Maryland, **2008**.

[28] Ayşe Deniz Duyul. *Control of an underactuated system around a periodic orbit*. Master's thesis, Middle East Technical University, **2018**.

[29] H. Sandberg and E. Mollerstedt. Harmonic modeling of the motor side of an inverter locomotive. In *Proceedings of the 2000. IEEE International Conference on Control Applications. Conference Proceedings (Cat. No.00CH37162)*, pages 918–923. **2000**. doi:10.1109/CCA.2000.897585.

[30] Georgia Deaconu. *On the trajectory design, guidance and control for spacecraft rendezvous and proximity operations*. Theses, Université Paul Sabatier - Toulouse III, **2013**.

[31] Norman M Wereley and Steven R Hall. Frequency response of linear time periodic systems. In *29th IEEE conference on decision and control*, pages 3650–3655. IEEE, **1990**.

[32] Matthew S Allen. Frequency-domain identification of linear time-periodic systems using lti techniques. *Journal of Computational and Nonlinear Dynamics*, 4(4), **2009**.

[33] Yaguang Yang. An efficient lqr design for discrete-time linear periodic system based on a novel lifting method. *Automatica*, 87:383–388, **2018**.

[34] Émile Mathieu. Mémoire sur le mouvement vibratoire d'une membrane de forme elliptique. *Journal de Mathématiques Pures et Appliquées*, 13:137–203, **1868**.

[35] A. ALLIEVI and A. SOUDACK. Ship stability via the mathieu equation. *International Journal of Control*, 51(1):139–167, **1990**. doi:10.1080/00207179008934054.

[36] Edward U. Condon. The physical pendulum in quantum mechanics. *Phys. Rev.*, 31:891–894, **1928**. doi:10.1103/PhysRev.31.891.

[37] John Churchill and F Holmstrom. Electron motion in a periodic potential and a uniform d.c. electric field. *Physica Scripta*, 43:434, **2006**. doi:10.1088/0031-8949/43/4/012.

[38] *Stability Analysis and Controller Design for Linear Time Periodic Systems Using Normal Forms*, Dynamic Systems and Control Conference, **2020**. doi:10.1115/DSCC2020-3132. V002T38A001.

[39] Michael Athans. The role and use of the stochastic linear-quadratic-gaussian problem in control system design. *Advances in Computers*, **1971**.

[40] Chrisitan Jakobsen, J. Camino, and Ilmar Santos. Rotor-blade vibration control using a periodic lqr controller. **2013**. doi:10.5540/03.2013.001.01.0011.

[41] Brian D. O. Anderson and John B. Moore. *Optimal Control: Linear Quadratic Methods*. Prentice-Hall, Inc., USA, **1990**. ISBN 0136385605.

[42] Paolo Arcara, Sergio Bittanti, and Marco Lovera. Active control of vibrations in helicopters by periodic optimal control. *Proceedings of the 1997 IEEE International Conference on Control Applications*, pages 730–735, **1997**.

[43] Aamir Hashim Obeid Ahmed. Optimal speed control for direct current motors using linear quadratic regulator. *Journal of Science and Technology*, 14, **2013**.

[44] Majed D. Youns, Abdulla I. Abdulla, and Salih M. Attya. Optimization control of dc motor with linear quadratic regulator and genetic algorithm approach. *Tikrit Journal of Engineering Sciences*, **2013**.

[45] Huibert Kwakernaak and Raphael Sivan. *Linear optimal control systems / [by] Huibert Kwakernaak [and] Raphael Sivan.* Wiley Interscience, New York, **1972**. ISBN 0471511102.